CHAPTER

Strain-Induced Crystallization

15

Aitor Larrañaga, Erlantz Lizundia
University of the Basque Country (UPV/EHU), Bilbao, Spain

1. INTRODUCTION

A great variety of polymers are processed under intense flow fields (elongation, shear, or mixed) before they reach the final consumer [1]. It has been shown that during these processes, such as extrusion, film blowing, and spinning, molten polymer is exposed to external flow fields, affecting the final properties and morphology of the resulting products through stretching and orienting polymer chains when compared with the quiescent melts [2,3]. It is generally accepted that during the stretching of polymers new crystal forms could be induced [4], crystallization kinetics are accelerated by several orders of magnitude [5], and even morphological modifications from spherulites to shish-kebab or row-nuclei structures may occur [6].

More interestingly, the performance of polymeric parts could be markedly improved by stretching these materials during their processing. For instance, the good mechanical properties of vulcanized natural rubber (VNR) arise from its ability to be crystallized when subjected to extensional fields, which form new crystals embedded within amorphous regions. These crystalline regions act as fillers (from the point of view of composite materials), improving the tensile modulus and tear strength of VNR [7,8]. A shear-controlled orientation injection molding could improve the mechanical properties of isotactic polypropylene (i-PP) products through the development of shish-kebab morphology [9]. This possibility for fine-tuning the final morphological and physicomechanical properties of plastics by simple well-established processing technologies makes strain-induced crystallization (SIC) an ideal industrial approach to fabricate materials with upgraded performances.

Owing to its industrial and scientific relevance, great efforts have been carried out to understand the SIC behavior of polymers. Even though the experimental findings have been confirmed by different research groups, the exact molecular mechanisms occurring during the SIC of polymers are not completely understood. Therefore in this chapter we aim to summarize the current state of the art and offer the latest theories dealing with the mechanisms governing the SIC of polymeric materials. First, the molecular basis dealing with the SIC of polymers is discussed.

Crystallization in Multiphase Polymer Systems. http://dx.doi.org/10.1016/B978-0-12-809453-2.00015-3

Then, the changes induced in the crystalline structure (crystal form, lattice dimensions) are given. Finally, and based on the potential applications for developing new crystalline structures upon stretching, an up-to-date overview focused on the -industrial applications and achieved properties such as mechanical, barrier, and piezoelectricity are highlighted.

2. STRESS–STRAIN RELATION DURING SIC

When polymer crystallization is induced by flow elongation, the semicrystalline morphology is affected by the orientation. The most obvious effects induced during flow are ascribed to kinetic and morphologic aspects. This effect has been extensively studied for rubber materials, especially for natural rubber (NR), synthetic polyisoprene, polybutadiene, and isoprene-isobutylene rubber. On the contrary, styrene-butadiene rubber cannot be crystallized upon the application of extensional strain field [10–13]. This underlines the many effects that affect the SIC in polymers and the actual need to summarize the current state of the art in this field.

Overall, it is well established that the application of stress is considered to cause molecules to change from a coiled to an extended configuration causing molecular alignment in the stretching direction. To illustrate how SIC of polymers proceeds, the stress–strain relation provides a great deal of valuable information. In this sense, Fig. 15.1 displays a stress–strain plot of a synthetic polyisoprene together with two-dimensional (2D) and three-dimensional (3D) wide-angle X-ray diffraction (WAXD) patterns corresponding to different stretching stages [14]. Although as a general trend the stress increases with strain, the curve shows a slight decrease in stress at approximately a draw ratio (λ) of 4.5 (indicated by the black arrow). This point is attributed to the beginning of SIC, where the stress decreases by increasing the length of the molecules along the stretching direction [10]. Once the critical strain is achieved, the initially coiled chains are able to partially crystallize [15]. Therefore two well-defined regions are observed. First of all, at $\lambda \leq 3$, WAXD patterns show an amorphous halo. In this region, polymer chains are continuously oriented, although they do not form any crystalline aggregate. In any case, the polymer molecules align in the flow direction and are able to create small ordered regions (known as "orientation-induced nuclei") because of the occurring interactions between them [16]. As strain increases ($\lambda = 4$), some weak crystalline reflections are observed surrounded by a predominantly amorphous pattern. At this point, highly oriented defective strain-induced crystallites are formed as a result of the increasing interaction between ordered adjacent molecules, although these entities are not large enough to create a macroscopically noticeable strain hardening effect. As highlighted by the sharp reflections at $\lambda = 5$, further deformation leads to a development of crystallites that are highly oriented along the stretching direction, with reflections corresponding to a well-defined unit cell [17]. Despite this fact, still an amorphous halo is found, indicating the coexistence of oriented crystalline domains within an amorphous matrix. Upon stretching, the freedom of movement of

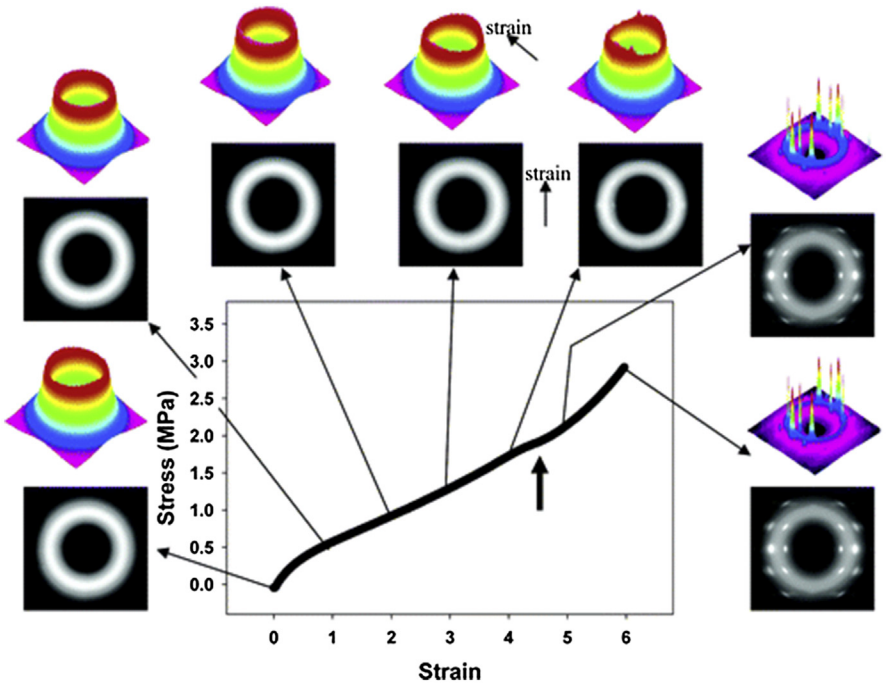

FIGURE 15.1

Stress–strain plot of a synthetic polyisoprene showing both 2D and 3D wide-angle X-ray diffraction patterns corresponding to different stretching stages.

Reproduced with permission of ACS Publications from Toki S, Sics I, Hsiao BS, Tosaka M, Poompradub S, Ikeda Y, Kohjiya S. Probing the nature of strain-induced crystallization in polyisoprene rubber by combined thermo-mechanical and in situ x-ray diffraction techniques. Macromolecules 2005;38:7064–73. http://dx.doi.org/10.1021/ma050465f.

polymeric chains decreases as a result of their orientation. Therefore molecules undergo a supercooled condition, which allows them to crystallize under low entropy barrier conditions [11]. In other words, amorphous molecules become part of the crystalline phase upon further stretching, and the overall crystallinity continuously increases by subsequent deformation. Finally, further deformation ($\lambda = 6$) increases the reflection's intensity as a result of the growth of an extended chain crystal network, where the majority of the chains are packed into crystalline regions. At this point, the strain-induced crystals are connected by amorphous regions, forming a physical network strong enough to withstand high stress values. Despite being counterintuitive, it is worthy to note that several works based on synchrotron studies have highlighted that, even though large strains are applied (up to 6), most of the chains may remain unoriented [13,18]. More precisely, from WAXD measurements, Toki et al. estimated the total mass fractions of isotropic and anisotropic phases [11].

About 75% of the isotropic fraction was obtained at the highest applied strain (the rest being composed by 20% of strain-induced crystallites and 5% of oriented amorphous phase), indicating that the vast majority of the molecules still remain in the random coil state under large deformations.

It is important to note that not only rubbers can be stretched to form new crystalline domains but similar behavior has also been found to occur in semiductile polymers such as polyethylene terephthalate (PET) and polyether ether ketone (PEEK). In the case of PET, the onset of strain hardening, and thus crystalline development, has been observed at $\lambda \approx 0.90$ [16] (at a strain of 1.4, a "perfect" fiber texture is achieved), whereas for PEEK the development of a nematic-like ordered regions (identified as the onset of strain hardening) has been observed to begin at $\lambda = 0.59$ [19]. In addition, other thermoplastics such as i-PP and poly(trimethylene terephthalate) (PTT) also present a shear strain threshold to induce conformational ordering [20,21]. It is important to underline that when semicrystalline brittle and semiductile polymers such as PET and polylactides (PLAs) are subjected to strain conditions [16,22], they need to be heated above their glass transition temperature (T_g) and below their cold crystallization temperature (T_{cc}) to ensure a more rubbery behavior. This temperature allows their processing by spinning or stretch-blow molding to orient their chains in their rubber-like state and is located between 90 and 120°C for PET and in the range 60−95°C for PLAs [16,22].

3. CHAIN RELAXATION, KINETICS, MORPHOLOGY, CHAIN CONFORMATION, AND EFFECT OF PROCESSING PARAMETERS

3.1 CHAIN RELAXATION

As a result of the supramolecular changes, chain relaxation of polymers is also affected upon stretching. To study these changes, Hernández et al. [15] used broadband dielectric spectroscopy (BDS) to investigate the influence of SIC on the chain relaxation features of NR. Depending on the applied strain λ, two well-defined regions were observed. In the first one, for strains lower than three, they found that, although stretching does not cause any crystallization, a dramatic increase of the dielectric strength (Δ_ε) from 0.2 to 0.8 occurs. They attributed this effect to the effective dipole moment increase upon stretching because chain ordering aligns the dipolar contributions that usually are cancelled in non-ordered amorphous polymers. Owing to the decreased free volume, this chain orientation induces an increase of both T_g (glass transition temperature) and T_0 (Vogel temperature, known as well as the ideal glass transition temperature and generally located 30−70°C below T_g) by ∼9°C, at the same time that the m fragility parameter (fragility is related to the way the temperature affects the molecular mobility of liquids above T_g, whereas m defines the apparent activation energy of relaxation time during the glass transition) increases because upon chain orientation more cooperativity is needed to

provoke segmental motions (according to the strong-fragile scheme proposed by Angell [23–25]). Conversely, the second region is observed at strains greater than three. Here, the newly developed crystalline regions slightly decrease the Δ_ε increase achieved at low λ because the dipoles are incorporated into crystalline phases and they do not contribute to the segmental relaxation process. In any case, the variation of both b and c shape parameters (which describe the symmetric and the asymmetric broadening of the equivalent relaxation time distribution function in the BDS) at high strains suggest a slight broadening of the relaxation for the segmental process as typically found upon polymer crystallization because the crystalline domains slow down the segmental dynamics [26].

Although the SIC has been widely studied for a great variety of polymeric materials, the relaxation following this orientation process has not been completely studied yet. It is known that the orientation degree achieved upon stretching is lost when the external force is removed because these oriented molecules tend to recoil into a more energetically favorable isotropic state. This effect is especially noticeable in the absence of crystals and entanglements or when high stretching temperatures and low deformation rates are utilized [27]. In this framework, Pearce et al. [28] and Matthews et al. [29] reported contradictory effects for uniaxially drawn PET. The former highlight that the relaxation is rapid at low stretch ratios; the latter state that at a low strain ratio the oriented molecules relax over long periods of time, whereas at high draw ratios this relaxation takes place faster. Hassan et al. [30] provide a rational for understanding these controversial relaxation effects in polymers crystallized upon stretching. In fact, the relaxation behavior of biaxially stretched PET as a function of stretching rate by Raman, differential scanning calorimetry (DSC), X-ray diffraction, and birefringence measurements was analyzed. It was found that the crystallinity and stress levels control the stress relaxation time in stretched PET. At low stretching values (regime I), the material remains amorphous and follows a linear quick relaxation with time because the chains retract free of constraints. At intermediate strains, in regime II, the initially amorphous but oriented chains begin to locally align upon relaxation, forming new crystalline domains. The formation of this connected physical network slows down the chain relaxation. For this to happen a minimum orientation degree before relaxation is a prerequisite. Finally, upon further stretching (regime III), the material is highly oriented and has already developed a well-connected physical network. At this point, the network is so constrained that is able to completely suppress the relaxation of oriented amorphous regions.

3.2 CRYSTALLIZATION KINETICS

Traditional plastic processing technologies require fast crystallization processes to shorten the time cycle needed for the production of consumer goods. Short cycle times reduce the time the material remains at high temperatures, decreasing the occurrence of undesired thermal degradation reactions and improving part quality. Moreover, materials displaying fast crystallization usually present better

dimensional stability in comparison with amorphous ones [31]. Taking advantage of the crystallization kinetic increase suffered by polymer systems such as polyolefins, polyesters, and polyethers when they are submitted to drawing [31,32], industry has been using SIC for a long time to shorten by several orders of magnitude the crystallization process in comparison with thermally induced crystallization [33]. For example, the crystallization kinetics of a blend consisting of i-PP of two different molecular weights could be increased by 10 times upon shear [34], whereas PET crystallization kinetics is drastically reduced from few minutes when it is thermally induced to 1−100 ms when it is stretched [35]. In this framework, this section deals with the underlying mechanism and the resulting effects of how the crystallization kinetics are affected by SIC.

One of the first works aiming to establish a link between crystallization kinetics and the applied strain/strain rate was carried out in the 1960s by Stein and coworkers [36]. Traditionally, the increase of crystallization kinetics has been attributed to an increase of nucleation rate induced by strain. If the applied field is strong enough, this nucleation enhancement is due to the entropy decrease in the polymer as a result of chain orientation upon stretching, which in turn decreases the nucleation barrier [37]. Most of the studies show that SIC occurs as a synergy between both short and long molecules [6,38]. For example, the crystallization of i-PP could be doubled by first growing a shear-induced oriented α phase, which serves as a starting nucleating point for the further growth of β phase [39]. Despite these remarkable works, very few studies have focused on SIC at the molecular level. Still several concepts remain ambiguous. For instance, although the existence of a preordered structure is widely accepted during strain, is that really necessary for the SIC? Do only long chains dominate the crystallization or is a synergy of short and long chains essential?

In this line, the work carried out by Tian et al. [40] provides new insights toward the complete understanding of the crystallization kinetic changes that occur upon SIC. In their work, they correlate the strain and nucleation rates in semicrystalline polymers by combining extensional rheology and in situ synchrotron small-angle X-ray scattering (SAXS) measurements. They found that the L long period decreases from 65 to 56 nm with increasing strain rate from 10 to 100 s^{-1}. This effect was ascribed to the incorporation of new crystals into the already existing lamellar stacks. Overall, they found a localized nucleation mechanism in which stretching leads to a sharp drop of the surface free energy in comparison with quiescent conditions, enhancing the nucleation rate. They attributed this effect to a smaller difference in conformation between melt and nuclei after deformation.

Several approaches have been reported for the quantitative interpretation of the flow-accelerated nucleation by combining polymer dynamics and nucleation theories [41,42]. A microrheological model where both polymer dynamics Doi−Edwards and crystallization Lauritzen−Hoffman theories are employed could explain the accelerated crystallization upon stretching [40]. Continuum models could also be utilized, where the macroscopic crystallization kinetics and the thermodynamics of the system need to be taken into account. Apart from that, an empirical relation between crystallization kinetics and applied strain/stress has been

provided by modifying the model proposed by Nakamura and coworkers [43]. Although these models are often used during industrial processes, they rely on processes that still remain open to debate [44]. Avrami theory, which describes how polymers transform from amorphous to crystalline phase with special emphasis in their kinetics, was used to evaluate crystallization kinetics from SAXS measurements. When i-PP was stretched up to small strains, Avrami exponents (n, which reflect the nature of the transformation) between two and three were obtained, suggesting the existence of disk-like and spherulitic crystals. As the polymer is further stretched, n decreases up to values of 0.5, indicating a transition to fibrillar/disk-like crystals first and to one-dimensional growth after. Similarly, crystallization half-time ($t_{1/2}$, the time required to achieve 50% of the final crystallinity of the samples) drastically decreases from 4000 to 45 s when a larger strain is applied (three regions with different kinetics are also identified depending on the applied strain). According to the experimental findings, Cui et al. [45] suggested a new crystallization model that properly explains the strong crystallization acceleration achieved. Accordingly, considering a polymer melt as an entangled network (Fig. 15.2A) [46,47], it may be supposed that under large viscoelastic deformations the interchain locking forces are overcome, resulting in the sliding of these entanglement points (chains become oriented, Fig. 15.2B). As shown in Fig. 15.2C, when the applied strain reaches the stress overshoot point, the network is fully disentangled. At this point, these flow-induced points rapidly create crystal nuclei or precursors (with no induction time)

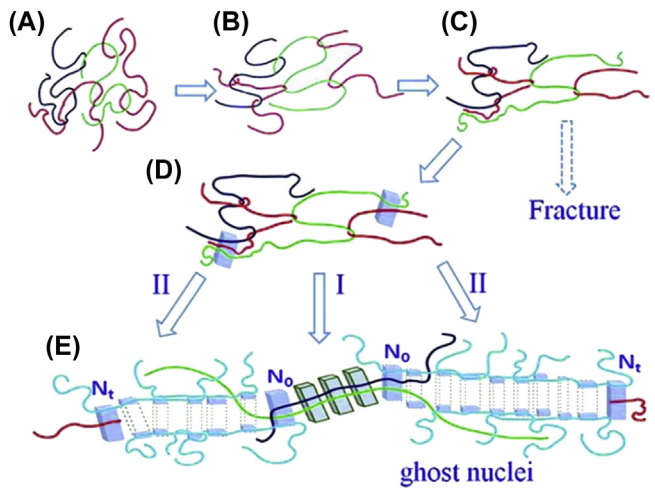

FIGURE 15.2

Schematic representation of the proposed "ghost nucleation" model in flow-induced crystallization of polymer melts.

Reproduced with permission of ACS Publications from Cui K, Meng L, Tian N, Zhou W, Liu Y, Wang Z, He J, Li L. Self-acceleration of nucleation and formation of shish in extension-induced crystallization with strain beyond fracture. Macromolecules 2012;45:5477–86. http://dx.doi.org/10.1021/ma300338c.

that act as physical cross-links within the deformed network, keeping it away from being fractured and resulting in the well-known strain-hardening effect (Fig. 15.2D). Here, two mechanisms are responsible for the accelerated crystallization. In the first one, identified as a self-acceleration, strain-induced nuclei act like locks on chains and become susceptible to form new precursors because of their lower nucleation barrier (stretched chain between N_0−N_0 points, Fig. 15.2E(I)) [48]. Second, a secondary nucleation exists as a result of a combination of self-epitaxial nucleation and flow effect (Fig. 15.2E(II)). At larger strains a gap could be formed between the nuclei and their surrounding macromolecules. These trails that are left behind, identified as N_0−N_f spaces, make the initial precursors to move along the path, inducing secondary nuclei through the left space. This mechanism was defined as "ghost nucleation" because the parent nuclei keep moving during the stretching of the polymer melt. Then, the daughter nuclei are detached from the parent ghost nuclei during extension. This hypothesis emerges as a plausible mechanism to explain the flow-induced orders increase of the nucleation and crystallization rate and is as well compatible with shish-kebab formation usually observed in polymer melts [6]. Therefore Cui et al. [45] suggested that the crystallization kinetics acceleration by several orders of magnitude and the shish formation are likely due to a self-acceleration effect by structural flow during strain rather than entropy loss of a simple polymer melt.

3.3 MORPHOLOGY CHANGES

When polymer crystallization is induced by flow elongation, the semicrystalline morphology is affected by the orientation. The most obvious effects induced during flow are ascribed to kinetic and morphologic aspects, where in comparison with quiescent conditions the developed crystals trend to evolve from spherical to elongated shapes. In this line, Fig. 15.3 roughly summarizes the typical morphologies achieved during polymer crystallization. Under static conditions, polymers crystallize into the typical spherulitic morphology (Fig. 15.3A). A weak elongation flow increases the presence of nuclei by orienting polymeric chains, leading to numerous elliptical crystallites aligned in the flow direction (Fig. 15.3B). Finally, upon large deformations crystallites are highly oriented and form a "shish-kebab" morphology (Fig. 15.3C) [37]. It is generally accepted that the application of stress causes the molecules to change from a coiled to an extended configuration, resulting in a molecular alignment in the stretching direction. In this section the most representative crystalline morphologies achieved upon SIC would be discussed.

The well-known shish-kebab crystalline structure was observed for the first time in the 1960s independently by Mitsuhashi, Pennings, and Binsbergen et al. [49−51]. Since then, a wide variety of works have been aimed to study both the underlying formation mechanism and the possibility of physicomechanical property improvement induced by this form. Despite these efforts, the shish-kebab formation is still unclear. The most accepted theory of shish-kebab formation upon stretching is based on the coil-stretch transition of polymeric chains proposed back in the 1970s by de

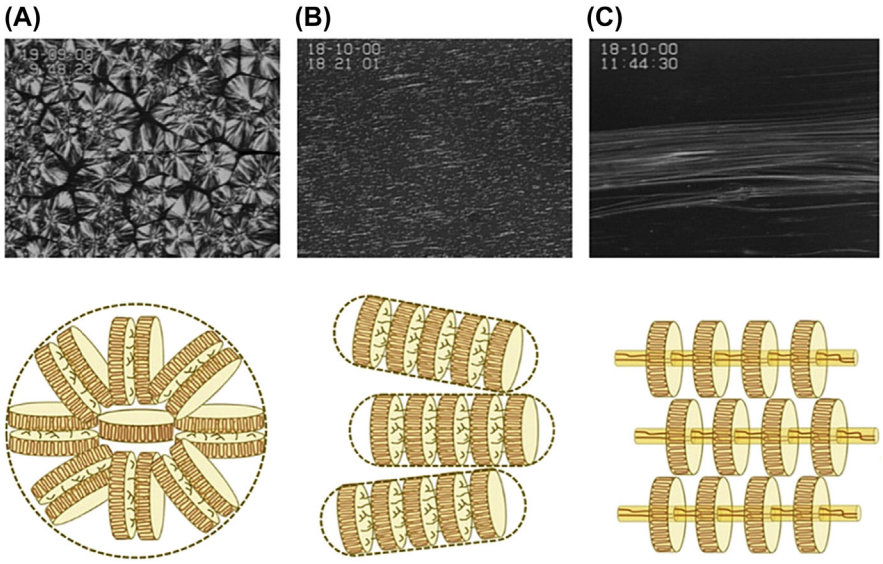

FIGURE 15.3

Typical morphologies achieved during polymer crystallization: quiescent conditions (A), under weak elongation flow (B), and under strong flow (C).

Reproduced with permission of ACS Publications from Wang Z, Ma Z, Li L. Flow-induced crystallization of polymers: molecular and thermodynamic considerations. Macromolecules 2016;49:1505–17. http://dx.doi.org/10.1021/acs.macromol.5b02688.

Gennes for dilute solutions [52]. This conformation change is a first-order transition and occurs suddenly once a critical strain rate (ε_c) has been exceeded [53]. The concept introduced by Keller has been accepted by the scientific community for many years.

In this theory, Keller states that during the flow-induced crystallization of entangled polymer melts these chains are discriminated according to their relaxation times [54–56]. Because deformed long molecules need longer times to relax back into their nondeformed state than shorter chains, Keller states that only polymeric chains having a molecular weight above a critical point (critical molecular weight, M^*) would remain oriented after the cessation of an elongational flow, and the shorter chains rapidly relaxed back to the coiled state [57]. Thus the following relationship accounting for the elongation rate was proposed:

$$\varepsilon_c \propto M^{\beta} \tag{15.1}$$

where ε_c is the critical elongation rate, M the critical molecular weight, and β a factor [equal to 1.5 in the case studies carried out by Keller for polyethylene (PE)]. After the flow-induced orientation of a highly entangled structure in the melt state, the occurring extended-chain crystallization results in a shish structure, which, after

subsequent folding of further coiled chains, is surrounded by kebabs. For the sake of comprehension, both low- and high-magnification scanning electron microscopy images of an ultrahigh-molecular-weight PE having a shish-kebab structure are depicted in Fig. 15.4A and B, respectively, whereas a scheme highlighting the shish-kebab structure is constructed in Fig. 15.4C. In addition, an atomic force microscopy image of the shear-induced shish-kebab structure where the shear direction is horizontal is shown in Fig. 15.4D. The observed individual lamellae highly aligned along the shear direction could be identified as kebabs in the shish-kebab morphology (note that the kebabs are so compact that the shish is not noticeable) [58].

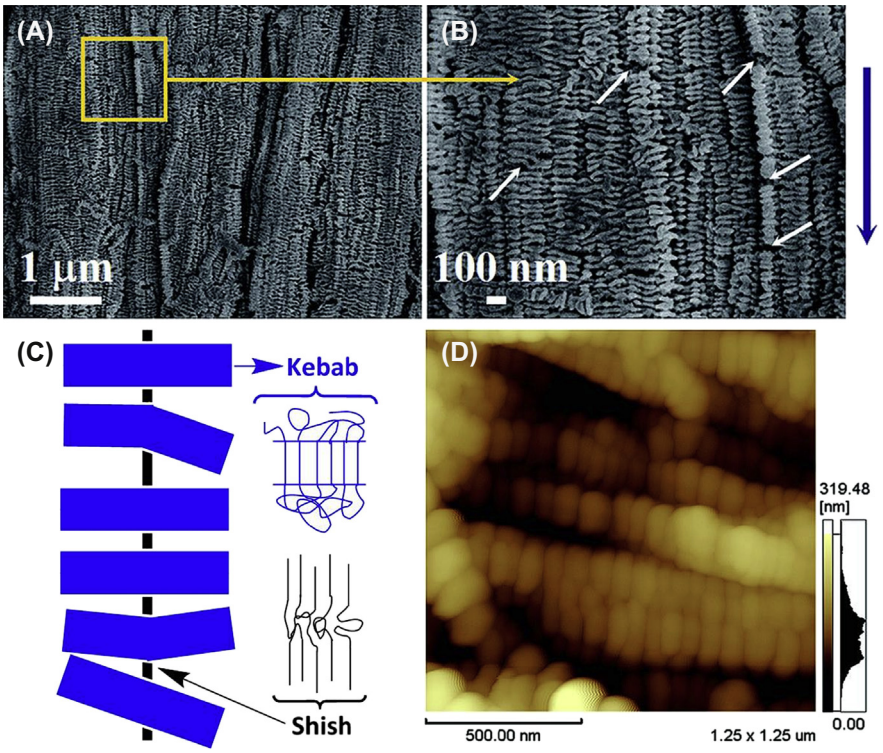

FIGURE 15.4

Scanning electron microscopy images of ultrahigh-molecular-weight polyethylene having a shish-kebab structure [*blue arrow* (black in print versions) refers to the shear direction] (A and B); (C) scheme highlighting the shish-kebab structure; and (D) an atomic force microscopy image of the shear-induced shish-kebab structure (the shear direction is horizontal).

Reproduced from Zheng H, Quan Y, Zheng G, Dai K, Liu C, Shen C. Fabrication of a polymer/aligned shish-kebab composite: microstructure and mechanical properties. RSC Adv 2015;5:60392–400. http://dx.doi.org/10.1039/C5RA07453C with permission from The Royal Society of Chemistry.

In analogy with Keller's observations, and based on WAXD, SAXS, and transmission electron microscopy observations, more recently Somani et al. [39] defined the concept of "critical orientation molecular weight" (M^*), which accounts for the minimum required chain length that allows the molecular orientation at a given shear rate. In any case, Keller did not take into account the fact that large chains cannot individually undergo stretch−coil transition because of the great number of chain entanglements, making difficult to completely explain the occurring SIC mechanism.

This long-standing concept has been disputed by several groups. For example, small-angle neutron scattering experiments have shown that the shish structure is composed of not only long chains but also short ones, which does not completely match with Keller's view [6]. In addition, rheo-SAXS experiments have demonstrated that coil−stretch transition is not a necessary condition for shish formation in polymers such as PE [59]. By combining in situ extensional rheological measurements (for the study of the coil−stretch transition) and synchrotron radiation SAXS (for shish/lamellar crystal formation analysis), Yan et al. concluded that the chains do not need to be stretched out from their original conformation for shish formation [59]. Therefore their experimental findings suggest that the stretched network plays a pivotal role on the formation of shish structure in polymer melts.

Keum et al. proposed a new hypothesis dealing with the formation of shish-kebab structures in entangled PE melts [60]. They performed their study with ultrahigh-molecular-weight polyethylene/high-density polyethylene (UHMWPE/HDPE) blends having very different molecular weights ($M_w = 5{,}000{,}000-6{,}000{,}000$ g/mol for UHMWPE and $M_w = 112{,}000$ g/mol for HDPE) because this allows having a blend composed by two constituents with relaxation times differing by an order of magnitude. A shear induced shish formation arising from UHMWPE chains was observed that at 142°C, while at 132°C the kebab-growth is diffusion-controlled rather than nucleation-controlled. Moreover, it was observed that kebabs were melted at 140°C, whereas shish structures where melted at 145.5°C. This suggests that kebab stability is dominated by the thermodynamics of coiled chains, whereas shish structures thermodynamics are controlled by stretched chains, which after their confination could not freely relax during their melting, resulting in a higher melting temperature (T_m). Overall, it was concluded that during the flow-induced crystallization, the highly entangled chains of a supercooled polymer could form a stable and entangled oriented network composed by both stretched and coiled molecules, implying that the chains do not need to undergo stretch−coil transitions. Subsequently, the stretched chains could undergo crystallization through extended-chain mechanism to yield shish structures at the same time that coiled segments suffer folded-chain crystallization, forming kebabs [61]. High-molecular-weight species would dictate the final topology of the crystalline structures, the concept M^* defined by Keller and still valid in this approach. In any case, for the determination of the exact physical meaning of M^* further studies are required.

It is known that the SIC of semicrystalline polymers involves orientation of the polymeric chains and the subsequent development of new crystalline phases or the

deformation of the already existing structures. In this framework, Okamoto et al. [62] reported that two mechanisms govern the final morphology of stretched polyethylene naphthalate (PEN). At low temperatures (170°C), a spherulitic morphology is mainly found because it keeps growing during deformation. As the stretching increases the already existing spherulites are deformed, where the stacked crystalline lamellae form an angle of about 45 degrees with the direction of elongation. On the contrary, at high temperatures the spherulites are unstable and the unfolded chains could then reorganize into extended-chain crystallites oriented along the deformation axis. It has been shown that in the shish-kebab morphology, the kebab is formed by lamellae that grow radially outward from the central shish until they impinged with each other [63].

A remarkable work carried out by Seki et al. showed the effect of long chains in shear-induced crystallization of high-molecular-weight i-PP blended with a metallocene i-PP having lower molecular weight [64]. In situ rheooptical measurements reveal that long chains prompt the transition from random to oriented growth, with only 1% of long chains being enough to induce remarkable crystallization modifications. As schematically depicted in Fig. 15.5, a propagation mechanism from a

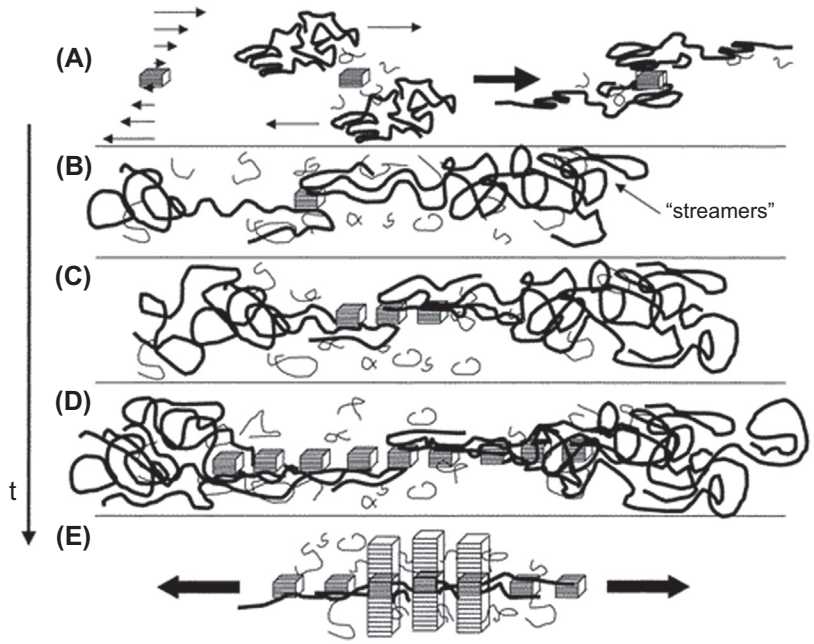

FIGURE 15.5

Schematic diagram depicting the mechanism of the shear-induced nucleation/growth of isotactic polypropylene blends composed of long and short chains.

Reproduced with permission of ACS Publications from Seki M, Thurman DW, Oberhauser JP, Kornfield JA. Shear-mediated crystallization of isotactic polypropylene: the role of long chain-long chain overlap. Macromolecules 2002;35:2583–94. http://dx.doi.org/10.1021/ma011359q.

thread-like precursor to a point-like precursor during SIC of i-PP blends was suggested. Initially, a long chain adsorbs to an existing point-like precursor upon elongation as a result of sustained shear (A). Then, as deformation increases, additional chains would adsorb to the long chain, leaving behind some dangling segments from "streamers" (B). The increased local orientation enhances the probability of adsorbing more segments (C and D), leading to lateral lamellar growth from the threadlike precursor, which induces the formation of a highly oriented growth with a shish-kebab−type structure (E). Overall, results indicate that the role of long chains during crystallization is a cooperative rather than a single chain effect, which is further enhanced by long chain−long chain overlap.

Varga et al. [65] showed an epitaxial growth of folded chain lamellae perpendicularly arranged to the already existing microfibrillar bundles during the shear-induced crystallization of i-PP. These supramolecular structures having cylindrical symmetry are known as cylindrites and have been achieved even at small shearing forces [51]. So, crystallized i-PP consists of a polymorphous mixture of α and β crystals located in the row-nuclei and cylindrites, respectively (Fig. 15.6) [66].

3.4 CHAIN CONFORMATION AND ORIENTATION

3.4.1 During Strain-Induced Crystallization

It would be expected that during SIC the macromolecular rotation and alignment from an isotropic state to an ordered state would modify the initial internal chain conformation. During this process, polymeric chains tend to order themselves into a lower energy conformation. Fourier transform infrared (FT-IR) spectroscopy has been mainly used to investigate the conformational changes thanks to its sensitivity to crystalline phases having different intermolecular interactions [67]. In the case of PE, this lower energy conformation is identified as an all-zigzag crystalline structure where every C−C bond is arranged into a *trans* mode [68]. Several works have shown that SIC is also able to modify the chain conformation of polymers because of the reorganization of macromolecules.

In this framework, during PET stretching the amount of glycol groups having a *gauche* conformation decreases as a result of chain extension and a decrease of non-oriented amorphous regions [69]. At the same time, an increase of *trans* configuration is observed because of the development of highly oriented amorphous phase and small oriented crystals [70]. When PLAs are uniaxially stretched, a decrease in the amount of amorphous *gauche-gauche* conformers (at 1777 cm^{-1} in the splitting in the second derivative of the carbonyl stretching band) together with an increase in the fraction corresponding to *gauche-trans* conformer (1759 cm^{-1}) is observed [22]. Similarly, it is shown that during PTT drawing immediately above T_g the chains having *gauche* conformation (band centered at 1358 cm^{-1}) increase at expenses of more amorphous *trans* conformation (976 cm^{-1}). This conformation change of methylene segments has been found to depend on the strain rate, and is faster as the polymer is subjected to faster strains [71]. In the same way, when polybutylene terephthalate and poly(butylene naphthalate) are strained, the initial

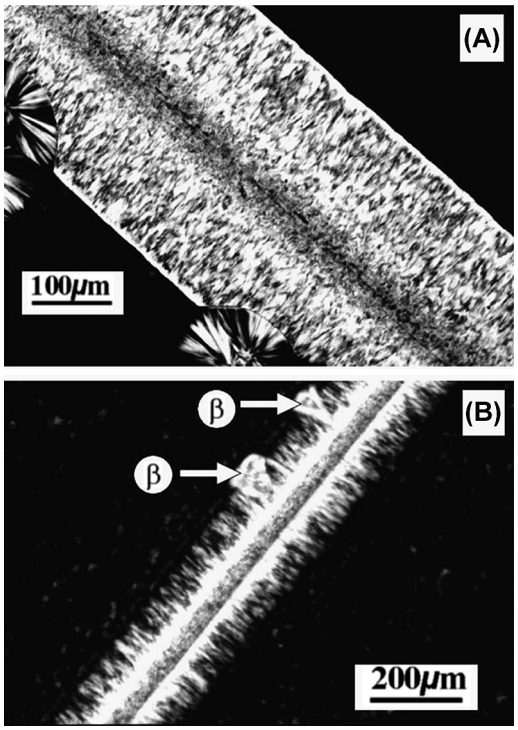

FIGURE 15.6

Evidence for cylindrite formation on row nuclei. (A) Optical micrographs of the i-PP fiber/matrix composites prepared by introducing the same i-PP fiber into a molten i-PP matrix and (B) subsequently isothermally crystallized at 138°C for 2 h.

Reproduced with permission of ACS Publications from Sun X, Li H, Zhang X, Wang D, Schultz JM, Yan S. Effect of matrix molecular mass on the crystallization of β-form isotactic polypropylene around an oriented polypropylene fiber. Macromolecules 2010;43:561–4.

gauche conformers are switched into *trans* conformers [72]. As a general rule, under external stresses, longer repeating length per monomeric unit along polymer chains is achieved, resulting in a transition from *gauche* conformers to *trans* conformers [72].

Because of the induced deformation, it may be expected that the unit cell dimensions of polymers are changed upon stretching, although contradictory results have been reported. For instance, it has been shown for PTT that after $\lambda = 0.25$ the *d*-spacing (also known as interplanar spacing and referring to the distance between adjacent *hkl* lattice planes) of the (002) plane increased, whereas the (010) spacing decreases. These changes correspond to the elongation of the *c* axis and the contraction of lateral dimension of the cell, respectively, and were attributed to the internal rotation of the methylene group to yield an elongated unit cell [73]. On the contrary,

based on 2D WAXD simulations and comparison with observed data, it has been suggested that the unit cell dimensions of both unvulcanized NR and synthetic polyisoprene rubber do not change when they are deformed at −50°C [74]. More precisely, as shown in Fig. 15.7, the average number of unit cells per crystallite has been found to be 4 × 4 × 4, whereas unit cell dimensions in the *a*, *b*, and *c* directions (L_{200}, L_{120}, and L_{002}) were found to be 5.51 × 3.12 × 3.00 nm, respectively. These a priori counterintuitive findings demonstrate the need of further research in this field to completely establish the effect of SIC on the atomic-scale features of crystallized polymers.

Another interesting effect is to analyze how chains are tilted or oriented upon SIC. When PET was stretched beyond the strain hardening region, Keum et al. observed a transient structure where the (001) *d*-spacing was determined to be ∼10.4 Å, nearly matching the monomer unit length (10.75 Å) of PET [75], suggesting the formation of locally densified bundles with chains arranged in parallel [76]. So as to accommodate more strain, new units are joined into the transient bundles, intensifying the (001) plane reflection upon deformation. Based on WAXD, modulated differential scanning calorimetry, and FT-IR spectroscopy findings, Keum and coworkers concluded that the fact that the layer spacing is shorter than the chemical repeat distance of PET was attributed to the presence of tilted chains (against the fiber axis) within layers [75].

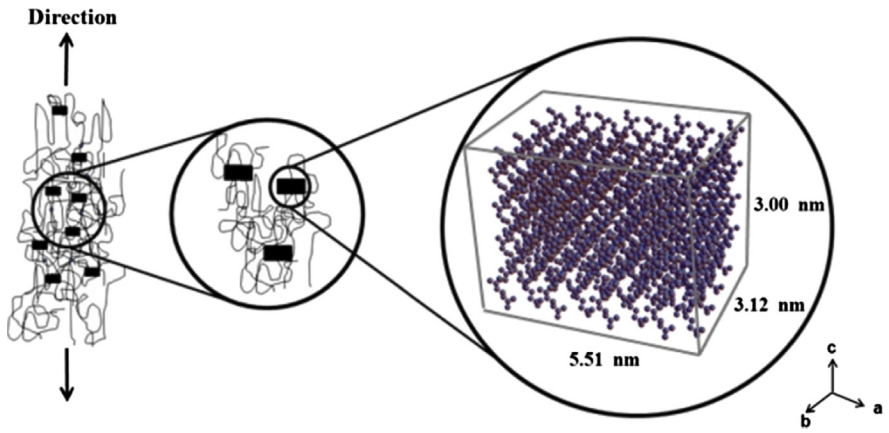

FIGURE 15.7

Scheme showing the estimated average crystallite size for unvulcanized natural rubber obtained upon strain-induced crystallization.

Reproduced with permission of ACS Publications from Che J, Burger C, Toki S, Rong L, Hsiao BS, Amnuaypornsri S, Sakdapipanich J. Crystal and crystallites structure of natural rubber and synthetic cis-1,4-polyisoprene by a new two dimensional wide angle x-ray diffraction simulation Method. I. Strain-induced crystallization. Macromolecules 2013;46:4520–8.

3.4.2 Strain-Induced Crystallization Versus Temperature-Induced Crystallization

During temperature-induced crystallization (TIC), polymer chains crystallize over time under static conditions. The energy pathway from the T_m melting temperature to the T_c crystallization temperature determines the crystallization kinetics of the process [77]. On the contrary, during SIC the entropy of the material is reduced by deformation and the amorphous-to-crystalline transition occurs as a result of the extensibility of the chains [10,78]. The crystallites are isotropically distributed through the material after TIC, whereas the crystallites developed during SIC are preferentially oriented with their crystallographic *c* axis parallel to the stretching direction. Moreover, TIC depends on the temperature and is a slow process (from seconds to hours depending on the system), whereas SIC is almost immediate and takes a few milliseconds [14].

Although the crystallinity fraction was about 33% lower when NR was crystallized by temperature than by stretching, Che et al. showed that the crystallite size and volume and the average number of unit cells per crystallite are larger when NR is crystallized by temperature [79]. Indeed, the volume of the crystallite achieved by TIC was found to be 502 nm^3, whereas for a given temperature, stretching-induced crystallization yields crystallites with an average volume of 34−81 nm^3. In the same way, work has shown that the crystalline domains formed upon PLA drawing (calculated according to Scherrer's equation) are of approximately 10−15 Å, whereas the crystallite size of thermally crystallized poly(L-lactide) (PLLA) are in the range of 61−75 Å depending on the crystallization temperature [22]. These differences were attributed to the variation in the crystallization rate between both processes. It is suggested that a stretched material crystallizes into smaller crystallites because the external constraints imposed during the drawing process do not allow the packing of macromolecules into large regular domains, whereas during TIC, the process takes place under static conditions where random crystalline regions are surrounded by amorphous phases.

Lizundia et al. [22] determined the 3D macromolecular orientation of PLA crystals induced by deformation using WAXD texture analysis via 2D pole figure measurements. As depicted in Fig. 15.8A, these results were compared with thermally developed isotropic PLA crystals (A), where no preferential orientation is observed. It can be seen in Fig. 15.8B that upon SIC, PLA crystals are preferentially orientated toward the stretching direction. Based on the obtained pole figures, a model depicting the strain-induced 3D crystal orientation was proposed as shown in Fig. 15.8C. According to the model, the externally imposed constraints upon stretching in both longitudinal and transversal directions decrease the number of degrees of freedom for crystallization process, avoiding the crystallization of 3D PLA crystals. Thus, while low stretching ratios result in few crystalline regions oriented along the MD axis (machine direction), an increase in the applied stress yields further crystalline domains arranged into planar spherulites that are oriented in the MD/ND plane (ND represents the normal direction along the thickness of the sample).

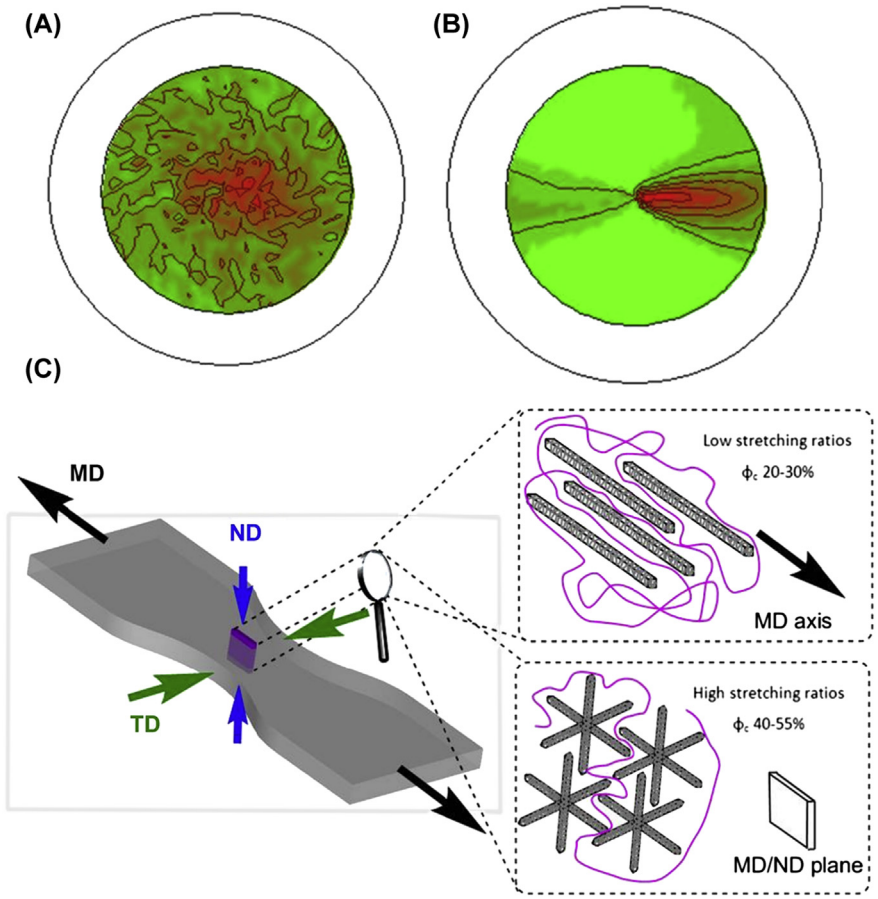

FIGURE 15.8

Obtained 2D pole figures (110)/(200) for poly(L-lactide) (PLLA) having the same bulk volume crystal fraction (~43%) for thermally crystallized material (A) and material crystallized upon stretching (B). Schematic representation showing the applied strain along three directions and the corresponding 3D crystal formation for low and highly stretched PLLA (C).

Reproduced from Lizundia E, Larranaga A, Vilas JL, Leon LM. Three-dimensional orientation of PLLA crystals under uniaxial drawing. RSC Adv 2016;6:11943–51 with permission of The Royal Society of Chemistry.

3.5 EFFECT OF PROCESSING PARAMETERS

Several works have highlighted that the obtained crystalline structure strongly depends on the stretching temperature. A polymer can be stretched (and thus crystallized by strain) and undergo the necking effect if the true stress–strain curve satisfies the Considère criterion [80]. For a rubbery material, this could be achieved at

temperatures as low as −20°C, although for a glassy brittle polymer such as PLA the above-mentioned condition is met when it is heated above its T_g [22]. Heating a polymer above the T_g involves brittle-to-ductile transition and decreases both drawing and yield stresses, improving the drawability of the material and allowing the high draw ratios that usually are required for industrial production.

However, the fact that the deformation temperature increases does not always mean that the SIC would be larger. This is the case of unvulcanized synthetic polyisoprene, which undergoes SIC at of −50, −25, and 0°C but not at 25°C. Toki et al. [81] explained this effect in terms of chain entanglements, which become pivots to align chains and induce crystals at relatively low temperatures, whereas at higher temperatures these entanglements disappear. Mahendrasingam et al. [82] showed a critical upper temperature bound of 125°C for PET (it easily crystallizes over the 85−125°C range). The fact that no crystallization was observed at high temperatures was explained in terms of the relaxation of the segment orientation, which is fast enough to prevent conditions suitable to orient polymer chains. Chuah et al. [83] provide another plausible explanation to this intriguing effect. For that end, PTT was used as a model polymer, which displays a semiductile behavior at room temperature and becomes rubbery with a strain at break of 600% at 50°C. However, it was found that when stretching was carried out at higher temperatures such as 75°C, PTT became ductile again and it cannot be crystallized by strain [83]. Therefore two opposing effects occur during the heating and subsequent stretching of semicrystalline brittle polymers. The temperature increase softens the materials through the brittle-to-ductile transition, whereas further temperature increase triggers cold crystallization events, stiffening the materials. Generally speaking, a maximum drawability is usually obtained at temperatures ranging from T_g to $T_g + 30$°C [83].

The deformation rate is one of the most relevant parameters in the SIC process of polymers. The deformation rate should be high enough to orient macromolecules, which further would develop the crystallization nuclei. The stability of these oriented chains is determined by the relaxation behavior of macromolecules, which is strongly correlated to their length and temperature [39]. When low strains are applied, even if they are applied at high rates, the induced orientation is not enough to form stable crystalline nuclei. On the contrary, at low strain rates, independently of the extent of the applied strain, the chains have sufficient time to relax, and therefore nuclei cannot be developed. In this sense, for a given strain, the amount of oriented chains is larger as shear rate increases [21]. Somani et al. quantified the amount of oriented i-PP for shear rates ranging from 10 to 102 s^{-1} at 140°C and observed that the oriented fraction was increased from ∼23% to ∼35% [39]. In any case, this issue should be carefully analyzed because a higher deformation rate does not always ensure a higher level of molecular orientation. Indeed, through atomistic level simulations of a model polymer it has been shown that during flow-induced crystallization, there is a critical shear rate from which the polymer does not further crystallize [84]. This upper limit of the shear rate (γ_c) is related with the reciprocal of the stress relaxation time ($\gamma_c \approx 1/\lambda$) and indicates the maximum

crystallinity that could be achieved for a given strain. Accordingly, high-molecular-weight polymers present this limit at lower shear rates because of the recoiling effect of large molecules.

In this respect, the period in which the strain is applied also influences the final crystalline morphology of stretched polymers. For instance, according to in situ rheo-SAXS and WAXD experiments, when i-PP is deformed under shear flow, both the amount of oriented crystal and the degree of crystal orientation (determined according to Herman's orientation function, *f*) are found to be larger when a short-duration shear at a high rate is applied rather than a long-duration shear at a low rate (the same macroscopic strain was applied because strain is the product of shear rate and shear duration) [4].

4. APPLICATIONS AND PROPERTIES

4.1 THERMAL TRANSITIONS

Physical properties of polymers are strongly related to their internal morphology such as the degree of crystallinity and orientation of the polymer chains in the amorphous phase. As previously discussed, stretching of polymeric samples induce both crystallinity (i.e., SIC) and orientation of the polymer chains. In this section, the effect of stretching on the observed thermal transitions of the polymers, which are closely linked to the above-mentioned characteristics, will be briefly discussed. The trend observed for most of the thermoplastic polymers reported in the literature is similar [85]. Herein, by way of example, the particular case of PLAs will be analyzed.

PLAs have attracted increasing interest as packaging materials and also in the biomedical field because of their biodegradability, biocompatibility, processability, and tunable mechanical properties. It has been reported that upon stretching, not only the intrinsic thermal transitions (i.e., glass transition, cold crystallization temperature, melting point) but also the developed crystalline structures of PLAs are affected [86]. At high drawing temperatures and/or high draw ratios, the formation of the β-crystal form is promoted in comparison with the α-crystal form, which is formed at lower drawing temperatures and/or ratios. Accordingly, the pseudoorthorhombic unit cell of the α-crystal form in PLLAs with dimensions a = 10.7 Å, b = 6.1 Å, and c = 28.8 Å where the molecules assume a -10_3 helical conformation can be transformed into the orthorhombic β-crystal form with dimensions a = 10.3 Å, b = 18.2 Å, and c = 9.0 Å, with molecules assuming a -3_1 helical conformation via SIC with controlled process parameters.

Regarding the thermal transitions, an increase in the T_g has been reported with increasing drawing ratios [87–89]. For instance, as shown in Fig. 15.9, through DSC heating thermograms, a T_g increase of 6.7°C has been reported when PLA is stretched by 340% [22]. This effect was ascribed to a chain confinement behavior induced by the decrease on the amorphous phase as the polymer is subjected to chain

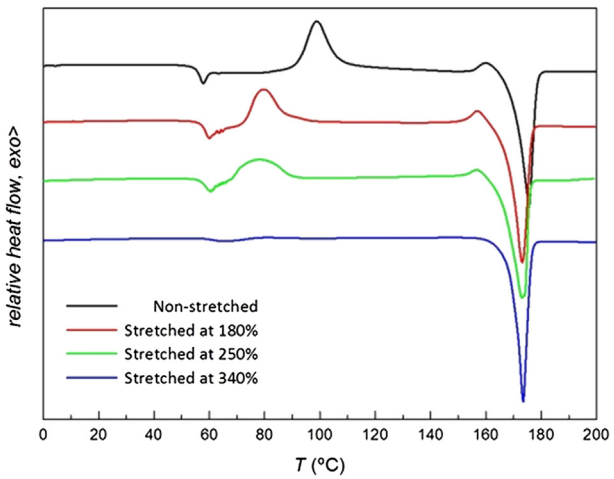

FIGURE 15.9

Differential scanning calorimetry heating thermograms of polylactide stretched at four different ratios (0%, 180%, 250%, and 340%).

Reproduced from Lizundia E, Larranaga A, Vilas JL, Leon LM. Three-dimensional orientation of poly(l-lactide) crystals under uniaxial drawing. RSC Adv 2016;6:11943–51. http://dx.doi.org/10.1039/C5RA22680E with permission of The Royal Society of Chemistry.

orientation through stretching (a limited mobility of the amorphous polymer chains that are close to those crystallites developed upon stretching is obtained). It has to be highlighted that a T_g increase up to 20°C for a draw ratio of eight has been reported, which may facilitate the use of this polymer in applications demanding improved mechanical performance at increased temperatures. Interestingly, this same effect was also reported for PLA samples subjected to plastic deformation by compression, suggesting that chain orientation is also possible in this type of mechanical deformation [90].

As observed in Fig. 15.9, a less marked cold crystallization peak is found as PLA is further stretched because of the continuous development of crystalline domains. More interestingly, it is observed that the T_{cc} moves toward lower values as the draw ratio increases. It seems that the higher degree of orientation of the polymer chains in the amorphous phase acts as nucleation points that facilitate the subsequent crystallization, resulting in a decrease in this temperature. It is also important to highlight that an endothermic peak, which increases with the draw ratio, appears just after the glass transition. This peak is associated with a relaxation enthalpy of the amorphous phase and suggests more oriented polymer chains.

To understand the mechanism of deformation of the amorphous and crystalline phases, more detailed studies have been carried out by means of FT-IR spectroscopy and/or WAXS. The orientation of the amorphous polymer chains appeared to be more effective at lower drawing temperatures, when chain relaxation is hindered

by the low mobility of chains at low temperatures [88]. In contrast, the orientation of the crystalline phase is more effective at increasing temperatures because the transformation from lamellar to microfibrillar structure is facilitated [89]. The discussion presented so far considers a simple two-phase crystalline-amorphous model, which has been demonstrated to be inadequate for most semicrystalline polymers. For semicrystalline polymers, a three-phase model [crystalline phase, mobile amorphous phase (MAP), and rigid amorphous fraction (RAF)] appeared to be more appropriate to describe the isotropic microstructure [91]. In this model, the RAF is composed of polymer chains in the amorphous phase that show limited mobility due to their proximity to the crystalline lamellae. A detailed analysis of the RAF with the drawing ratio revealed that RAF was closely linked with the crystalline fraction. In this sense, RAF appeared for a draw ratio of 2.5 for PET, which is also the draw ratio at which the crystalline phase appeared. In contrast to RAF, the orientation of MAP occurred independently of crystal formation. Accordingly, the orientation of MAP was observed from the first stage of drawing, even below the limit at which the strain-induced crystalline phase was developed. To sum up, it can be concluded that the internal morphology of polymers (degree of crystallinity and orientation), which is reflected in the observed thermal transitions, is clearly affected by their processing history such as mechanical deformations. These mechanical deformations result in important changes in the final properties (e.g., mechanical properties, degradation rates, optical properties) of the materials and need to be considered for the specific applications.

4.2 MECHANICAL PROPERTIES

It is well reported that mechanical drawing is an established strategy to yield polymeric materials with improved mechanical properties, in terms of Young's modulus and tensile strength. Tensile drawing, solution spinning, and drawing of gel-spun fibers are only few of the examples that can be found in industrial processes to produce polymer fibers and films with ultrahigh mechanical performances. Several process parameters such as the molecular weight of the polymers, drawing temperature, drawing ratio, and thermal treatments determine the effectiveness of the drawing process.

In the particular case of PE, theoretical calculations determined that the moduli for the fully extended PE chains should be around 240 GPa. In some studies, extensional moduli up to 70 GPa have been reported, with the moduli being strongly dependent on draw ratio [92]. In contrast, the effect of molecular weight and molecular weight distribution on the final mechanical properties of PE was almost negligible. In this sense, a PE sample of $M_n = 6.180$ g/mol and $M_w = 101.450$ g/mol showed a very similar trend of the extensional moduli with a draw ratio with respect to a sample of $M_n = 13.350$ g/mol and $M_w = 67.800$ g/mol up to a draw ratio of 30. As observed in Fig. 15.10, the extensional modulus linearly increased with the draw ratio for both PE samples. In this sense, the extensional modulus was $\sim$35 GPa for a draw ratio of 21 and $\sim$69 GPa for a draw ratio of 30, which shows a linear

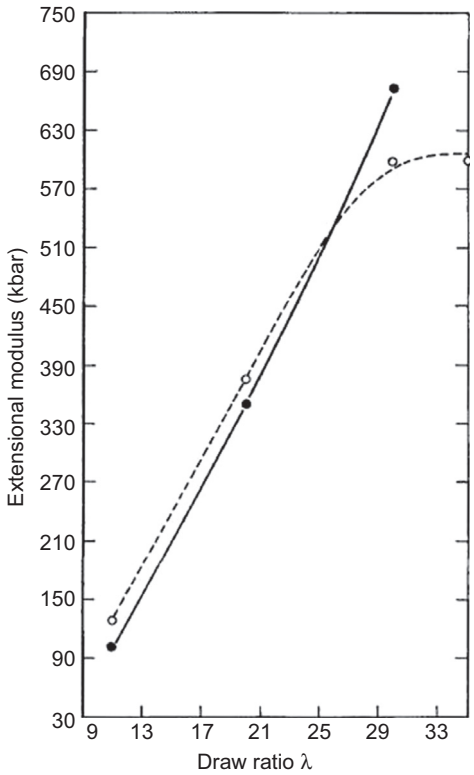

FIGURE 15.10

Extensional moduli versus draw ratio for polyethylene samples of $M_n = 6.180$ g/mol and $M_w = 101.450$ g/mol (*solid line*) or $M_n = 13.350$ g/mol and $M_w = 67.800$ g/mol (*dashed line*).

Reproduced with permission of Nature Publishing Group from Capaccio G, Ward IM. Properties of ultra-high modulus linear polyethylenes. Nat Phys Sci 1973;243:143.

correlation between the extensional modulus and draw ratio. However, the molecular weight and its distribution did affect the structural properties of the studied PE samples [93]. The sample with lower M_w ($M_w = 67.800$ g/mol) and lower polydispersity index showed a melting peak of 138.5°C, indicating the presence of extended chain crystallites upon drawing. These mechanical properties suggest that the presence of extended chain crystallites was not necessary to yield PE with an ultrahigh modulus, playing the oriented noncrystalline extended chains (tie molecules) a major role in the final mechanical properties of the polymer.

Hallam et al. [94] also reported that the molecular weight and its distribution had negligible effect on the modulus of PE samples subjected to mechanical drawing. However, the recorded tensile strength linearly increased with decreasing polydispersity indexes, resulting in polymers with improved tenacity. For example, for a

given draw ratio (e.g., 20), the tensile strength for a PE sample having $M_w = 101{,}000$ g/mol and a polydispersity (M_w/M_n) of 8.2 was 0.94 GPa, whereas for a PE sample with similar M_w (100,000 g/mol) but decreased polydispersity index ($M_w/M_n = 7.7$) the tensile strength was 1.16 GPa. In the same study, the effect of the drawing temperature on the tensile strength of the samples was also analyzed. At a given temperature, the tensile strength increased with the draw ratio up to a maximum and then declined. The decline in the tensile strength with the draw ratio was observed before for those samples that were drawn at lower temperatures. It was hypothesized that the decline in the tensile strength was associated with the formation of microvoids, which is favored when drawing was performed at lower temperatures. From this study, it was concluded that to achieve ultrahigh mechanical properties a high-molecular-weight polymer with a low polydispersity index, high draw ratio, and high draw temperature was preferable.

From the studies mentioned earlier, it can be deduced that the molecular weight and molecular weight distribution have little effect on the moduli of the obtained materials. However, it has to be considered that these parameters may affect the draw ratio achievable at a fixed draw ratio and draw temperature [95], which, in fact, will indirectly affect the final modulus. In this sense, a similar maximum draw ratio ($\sim$40) was achieved for two PE samples with different molecular weights and distribution (Alathon 7030: $M_w = 93.700$ g/mol/$M_n = 22.000$ g/mol; LP 51.1: $M_w = 208.000$ g/mol/$M_n = 11.000$ g/mol). However, the temperature at which the maximum ratio was achieved clearly differed between these two polymers (Alathon 7030: 60°C; LP 51.1: 100°C). As a result, for the same maximum draw ratio ($\sim$40), LP 51.1 was drawn at a higher temperature than Alathon 7030 (100 vs. 60°C) and the resulting modulus was higher because of a better alignment of longer chains achieved at higher temperatures.

The fabrication of PE films with an even higher modulus was attempted by biaxial drawing [96]. Up to a draw ratio of 10, biaxial stretching was as effective as uniaxial drawing in terms of Young's modulus improvement. However, above this threshold, biaxially oriented samples showed a lower modulus than uniaxially oriented ones, indicating the lower effectiveness of biaxial drawing. Apart from the above-mentioned standard drawing processes, other techniques such as extrusion through a capillary are commonly employed to achieve polymer samples with ultrahigh mechanical performance [97]. In this case, draw ratios up to 300 can be obtained that produce stressed chains and increased crystalline alignment.

Similar studies have also been conducted with several polymers [e.g., i-PP, PLA, polyoxymethylene (POM)] [98,99] and, again, the influence of process parameters and material characteristics on the final mechanical properties was highlighted. In the case of POM, for example, the effect of single-stage or two-stage drawing on the mechanical properties was studied. Several parameters of the second stage were modified, such as draw rate or draw temperature. However, none of these parameters resulted in an improvement of the mechanical properties of POM samples in comparison with a single-stage drawing, indicating that there is no advantage to be gained from two-stage drawing.

Studies on PLAs have gained particular interest for biomedical applications. This biodegradable and biocompatible material represents a promising alternative to metals and ceramics that are widely used as orthopedic fixation devices. However, the mechanical properties of PLAs are below those of cortical bone, limiting their application for load-bearing applications. Via the hydrostatic extrusion technique, improved bending strength and modulus were obtained in comparison with samples subjected to uniaxial deformation, thanks to the absence of crystal voids and cracks in the sample [100]. Accordingly, bending strength was improved from 125 MPa for a draw ratio of one to 340 MPa for a draw ratio of eight. Moreover, these samples preserved better the mechanical properties during a degradation study.

4.3 BARRIER PROPERTIES

Polymers have gained increasing interest for their use as packaging materials for foods and beverages and accordingly represent a current substitute to more traditional alternatives such as glass or metals. Ideally, a barrier material for packaging should hinder the interaction of the product with the environment because even the diffusion of a small amount of oxygen, carbon dioxide, water vapor, aromas, etc. may deteriorate the product taste. Among the available polymeric materials for packaging, PET has been widely employed because of its low price and good mechanical properties. However, PET shows intrinsically poor barrier properties in its amorphous, isotropic, unprocessed form. Therefore several strategies have been considered to improve the barrier properties of PET and allow its safe use as packaging material. Copolymerization with isophthalate, phthalate, or naphthalate, in which the linear terephthalate unit is replaced with a kinked isophthalate or phthalate group, has been demonstrated to reduce the solubility and diffusivity of oxygen upon cold crystallization [101]. This effect was associated with a different tendency of the amorphous phase of PET to densify during the cold crystallization process. Instead of copolymerization, blending with polymers of lower gas permeability, such as poly(ethylene isophthalate) [102], poly(m-xylene adipamide) (nylon-MXD6) [103], or PEN [104], has also been employed as an efficient strategy to reduce the overall permeability of the resulting material. In the case of PET/PEN blends, it has to be first considered that PEN shows air permeation four to five times lower than that of PET. In addition, upon biaxial orientation of PET/PEN containing PEN concentration equal to or less than 30%, phase-separated PEN parallel layers are developed within the PET matrix forming multilayer microstructures that greatly improve the barrier properties of the resulting material. Finally, incorporation of impermeable high aspect ratio flakes or platelets (e.g., talk platelet particles) can also be employed to improve the gas barrier properties of PET [105]. Herein, the effects of stretching in the final barrier properties of PET will be described.

To understand the transport of gases through a polymeric material, two fundamental factors have to be considered. On the one hand, gas solubility (S) measures the uptake of the gas molecules by the polymer and is related to the number and size of "holes" in the polymer matrix (static free volume), and is independent of

thermally accessible motions of the polymer chains. On the other hand, diffusion (D) is related to the speed at which a gas molecule diffuses through the polymer. This occurs when a channel is formed between two neighboring "holes" and thus depends on the frequency of channel formation (dynamic free volume), being related to accessible conformational changes and segmental motions of the polymer chains. The product of these two coefficients represents the overall permeability [106].

It is well accepted that crystalline regions in polymers do not allow the solubility of gas molecules [107]. Therefore solubility and subsequent diffusion of gas molecules takes place through the amorphous region of the polymer. Upon uniaxial or biaxial deformation of PET, the overall density of the polymer increases as a result of an increase in crystallinity fraction. Birefringence, which is related to the overall molecular orientation, is also enhanced in this process. In a first attempt to predict the diffusion of gases along the PET matrix, the Maxwell equation can be employed:

$$P\alpha\frac{(1-f)}{(2+f)} \tag{15.2}$$

where P is the permeability and f is the fraction of impermeable material. If f is considered as the fraction of crystalline phase in the polymer determined by density measurements (i.e., considering the polymer a simple mixture of crystalline and amorphous components with two different and constant densities), a good correlation between gas permeability and density (or crystalline fraction) is obtained [108]. From this perspective, it can be concluded that increasing the crystallinity fraction via stretching is a valid strategy to hinder the permeation of gas molecules along the polymeric material. However, crystallization is not the only process occurring during stretching. Orientation, which results in an increase in the *trans* fraction in both the crystalline and amorphous phases, occurs simultaneously and, as it will be discussed afterward, also plays an important role in the overall permeability of PET toward gas molecules.

Not only the degree of crystallinity but the morphology of the crystalline phase also affects the barrier properties of PET [109]. In thermally crystallized samples (not stretched), larger spherulites hinder the permeation of gases along the polymer matrix because of the greater tortuosity for the permeant molecules, suggesting that permeability is controlled by macrostructural parameters. However, in the case of stretched samples, microstructural parameters, determined by the fraction of molecules in the *trans* conformation, seem to play the major role.

So far, gas permeation has been discussed in terms of an impermeable crystalline phase and a permeable amorphous phase. Stretching can induce crystallization and accordingly reduce the permeability of gas molecules. But, as previously mentioned, there occur also conformational changes in the amorphous phase upon stretching that play an important role in the resultant barrier properties of the polymer. In this sense, the amorphous phase can be also subdivided into a permeable phase with ethylene linkages predominately in the *gauche* conformation and an impermeable amorphous phase with ethylene linkages that have transformed from *gauche* to *trans* during stretching [108,110,111]. Good correlations have been obtained

between the permeability of gases and the amount of *trans* fraction, highlighting the importance of this parameter in the overall barrier properties of the polymer.

Finally, the effect of dedensification of the amorphous phase on the barrier properties of PET will be briefly summarized. It has been reported that postprocessing of cold-drawn films and bottles of PET to increase the crystalline fraction detrimentally affects the barrier properties of the resulting material. This was associated with a dedensification process in the amorphous phase that occurs because of the constraint on amorphous chains that are attached to rigid chain segments in crystals [112,113]. As a result, the density of the amorphous phase decreases, allowing a better diffusion of gas molecules along the polymer.

4.4 PIEZOELECTRICITY

Poly(vinylidene fluoride) (PVDF) displays the highest dielectric constant and electroactive response among the polymeric materials, showing piezoelectric, pyroelectric, and ferroelectric properties. This is because each polymer chain possesses a dipole moment perpendicular to the polymer chain due to the high electronegativity of fluorine atom in comparison with hydrogen and carbon. Thanks to these features, PVDF has been satisfactorily applied as electrothermal and electromechanical transducer material in the field of sensor and actuator devices and technologies. PVDF is a semicrystalline polymer presenting intrinsic polymorphism, being able to crystallize in, at least, four crystalline phases (α, β, γ, and δ) [114] (Fig. 15.11). The α-phase ($TG^+ TG^-$) is the most common one and is obtained by melt crystallization at temperatures below 160°C. Crystallization at higher temperatures produces a

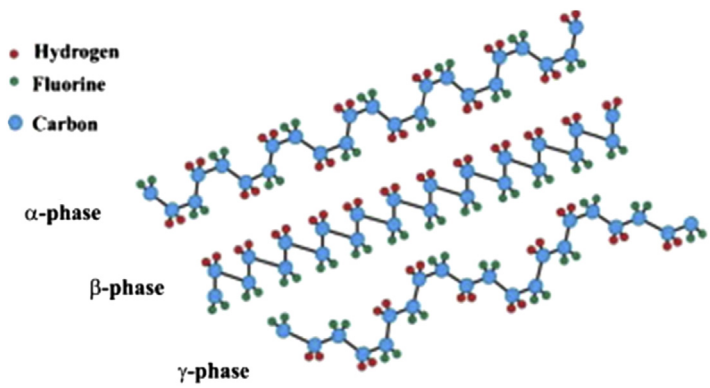

FIGURE 15.11

Chain conformation of the most commonly studied poly(vinylidene fluoride) crystalline phases.

Reproduced with permission of Elsevier from Martins P, Lopes AC, Lanceros-Mendez S. Electroactive phases of poly(vinylidene fluoride): determination, processing and applications. Prog Polym Sci 2014;39:683–706. http://dx.doi.org/10.1016/j.progpolymsci.2013.07.006.

mixture between the α- and γ-phase (GTTT), with more γ-phase at increasing temperatures and times.

However, from a technological point of view, β-phase is the one that has attracted more interest because it provides the best pyroelectric and piezoelectric properties. In this crystalline phase, the dipoles are oriented in parallel and, accordingly, the polymer presents a net dipole moment. For that reason, several strategies have been adopted to promote the content of β-phase in PVDF, such as stretching from the α-phase, applying high pressure from the melt, ultrafast cooling, external electric field, addition of nucleating agents (e.g., $BaTiO_3$, ferrite nanoparticles, gold nanoparticles), and copolymerizing with trifluoroethylene [115]. Stretching from the α-phase at different temperatures and draw ratios is the most commonly adopted strategy [116–118] and is the one that will be discussed in this chapter.

To exploit the piezoelectric and pyroelectric properties of PVDF, the content of β-phase in the polymer needs to be first maximized. The amount of β-phase can be determined by several techniques, with X-ray diffractometry and FT-IR spectroscopy being the most widely employed ones [119]. The FT-IR spectra of the β-phase is characterized by the appearance of strong absorption bands at 510, 840, and 1279 cm^{-1}, whereas bands at 530, 614, and 796 cm^{-1} are characteristic of the α-phase. Accordingly, the content of each phase can be estimated by the ratio between the aforementioned absorption bands.

To maximize the content of β-phase, several parameters (e.g., stretching temperature, speed, draw ratio) in the stretching process have been thoroughly analyzed, with the draw ratio and the stretching temperature playing the major role. As depicted in Fig. 15.12A, the relative fraction of β-phase (F(β)) of PVDF sharply decreases for stretching temperatures above 100°C, highlighting the importance this parameter has in the resulting fraction of β phase. Several studies have determined that the transition from α- to β-phase occurs when the stretching is done below 130°C [121,122]. In this temperature range, the stress–strain curve of PVDF showed a defined yielding peak, followed by necking and strain hardening as strain increases. When necking occurs, appearance of β-phase was monitored by X-ray diffraction. In contrast, when the sample was stretched at 150°C, no yield point was detected in the stress–strain curve, resulting in no necking of the sample. In this case, no β-phase was detected in the X-ray diffractograms even at the highest drawing ratio ($\lambda = 5$).

On the other hand, the importance of draw ratio in the F(β) of PVDF is reflected in Fig. 15.12B. At the selected stretching temperature ($T_s = 100°C$) and speed ($V_s = 50$ μm/s), the F(β) of PVDF monotonously increases up to a $\lambda \sim 3$ and is maintained almost constant for $\lambda > 3$. In the case of stretching at high temperatures, draw ratios above the natural ratio were necessary to promote the transition from α- to β-phase [123]. In this sense, with a draw ratio of 6.7, a material with superior mechanical properties and a content of β-phase exceeding 80% of volume was achieved.

Finally, the negligible effect V_s has on the F(β) of PVDF can also be concluded from Fig. 15.12B. In this sense, no significant differences are observed in the calculated F(β) when the V_s was increased from 1 to 1000 μm/s.

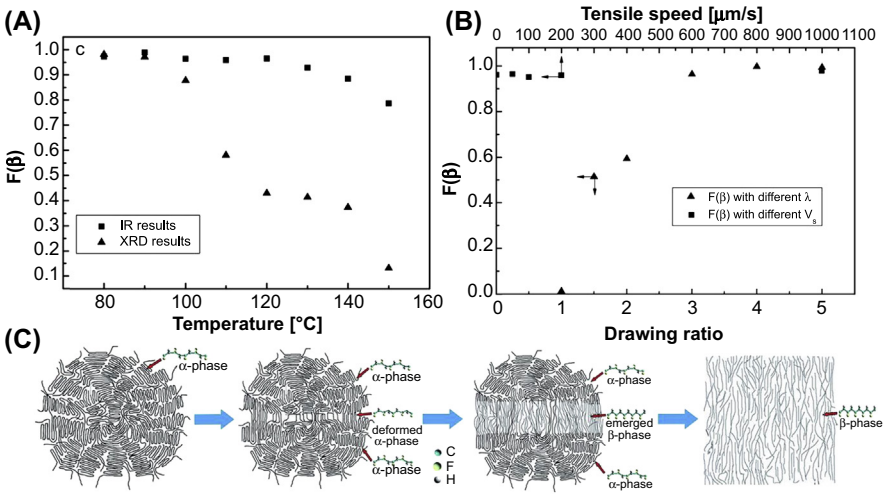

FIGURE 15.12

Relative fraction of β-phase (F(β)) of poly(vinylidene fluoride) (PVDF) stretched under (A) different temperatures (T_s) and (B) different tensile speeds (V_s)/draw ratios (λ). (C) Scheme showing the transformation process from α-crystal to β-crystal of PVDF upon stretching.

Reproduced from Li L, Zhang M, Rong M, Ruan W. Studies on the transformation process of PVDF from α to β phase by stretching. RSC Adv 2014;4:3938. http://dx.doi.org/10.1039/c3ra45134h with permission of The Royal Society of Chemistry.

The transformation process from α-crystal to β-crystal of PVDF upon stretching is shown in Fig. 15.12C. When the initial alpha spherulite having folded chains is stretched, the molecular chains begin to extend along the drawing direction from the middle of the spherulite. Upon further deformation, regions of extended chains expand transversely along the middle of the spherulite, where the entire spherulite of the α-phase is transformed into the β-phase under large deformation [120]. Overall, it can be concluded that crystal transformation happens when the sample undergoes cold drawing, with the heterogeneous stress component playing a critical role in this transformation. Even if stretching significantly increases the content of the β-phase in PVDF, the measured piezoelectricity is still low after mechanical deformation. Therefore a postprocessing step of poling is usually required to further increase the dipole orientation and the subsequent piezoelectricity [124].

As a consequence of increasing the content of β-phase in the polymer, the piezoelectric response of PVDF, which can be measured via a d_{33}-meter, can be clearly enhanced. In this sense, the maximum d_{33} value ($d_{33} = 34$ pC/N) was reported for a PVDF sample that underwent a draw ratio of 5 at a temperature of 80°C, showing this sample had the highest content of β-phase among the samples studied. For lower draw ratios or higher temperatures, the content of β-phase as well as calculated d_{33} gradually decreased, indicating a clear proportionality between the content of β-phase and the piezoelectric response of PVDF [125].

5. CONCLUSIONS AND PERSPECTIVES

This chapter aims to provide a general overview about the morphological changes that polymers undergo upon SIC. Most commonly employed industrial processes induce an external flow field within the polymer that results in the orientation of the polymer chains and, eventually, in the formation of strain-induced crystallites. All these changes in the internal morphology of the material are determined by the employed process parameters as well as by the intrinsic properties of the initial material. Crystallization kinetics during the SIC are greatly enhanced in comparison with quiescent conditions, where the time required for completing the crystallization process could be reduced from few minutes when it is thermally induced to 1−100 ms when it is stretched. Another interesting aspect is the morphological changes induced upon stretching, where the developed crystals evolve from spherical at low strain rates to elongated shapes and, upon further stretching, to highly oriented crystals known as shish-kebabs.

Accordingly, the final properties can be enhanced via SIC, providing a successful strategy to lead polymeric materials with advanced properties. For example, polymeric materials with ultrahigh elastic moduli (similar to those reported for some metals or ceramics) have been achieved via the precise control of the process parameter in the drawing process. On the other hand, barrier properties, which play a pivotal role when the polymer is intended to be used as a packaging material, can also be enhanced via SIC. In this particular case, the development of strain-induced crystallites, which show little or no permeability to molecules, together with the orientation of the polymer chains in the amorphous phase, decrease the overall permeability of the resulting material. Finally, in the case of PVDF, stretching promotes the polymorphic α- to β-phase transformation, which is a must for the development of PVDF-based materials with a piezoelectric response.

The examples provided earlier highlight the relevance of internal morphology on the final properties of the resulting polymeric materials. To understand how commonly employed industrial processes affect the internal morphology of the polymers, molecular basis and associated segmental dynamics, kinetics, and morphological and structural modifications have to be considered. Understanding all these concepts will allow the optimization of process parameters and intrinsic properties of the initial materials to yield polymeric materials with improved properties.

REFERENCES

[1] Lee O, Kamal MR. Experimental study of post-shear crystallization of polypropylene melts. Polym Eng Sci 1999;39:236−48. http://dx.doi.org/10.1002/pen.11410.

[2] Peterlin A. Drawing and extrusion of semi-crystalline polymers. Colloid Polym Sci 1987;265:357−82. http://dx.doi.org/10.1007/BF01412215.

[3] Drumright RE, Gruber PR, Henton DE. Polylactic acid technology. Adv Mater 2000; 12:1841−6. http://dx.doi.org/10.1002/1521-4095(200012)12:23<1841::AID-ADMA1841>3.0.CO;2-E.

[4] Avila-Orta CA, Burger C, Somani R, Yang L, Marom G, Medellin-Rodriguez FJ, Hsiao BS. Shear-induced crystallization of isotactic polypropylene within the oriented scaffold of noncrystalline ultrahigh molecular weight polyethylene. Polymer (Guildf) 2005:8859–71. http://dx.doi.org/10.1016/j.polymer.2005.05.136.

[5] Kumaraswamy G, Kornfield JA, Yeh F, Hsiao BS. Shear-enhanced crystallization in isotactic polypropylene. 3. Evidence for a kinetic pathway to nucleation. Macromolecules 2002;35:1762–9. http://dx.doi.org/10.1021/ma0114180.

[6] Kimata S, Sakurai T, Nozue Y, Kasahara T, Yamaguchi N, Karino T, Shibayama M, Kornfield JA. Molecular basis of the shish-kebab morphology in polymer crystallization. Science 2007;316:1014–7. http://dx.doi.org/10.1126/science.1140132.

[7] Zhang HP, Niemczura J, Dennis G, Ravi-Chandar K, Marder M. Toughening effect of strain-induced crystallites in natural rubber. Phys Rev Lett 2009;102. http://dx.doi.org/10.1103/PhysRevLett.102.245503.

[8] Le Cam JB, Toussaint E. The mechanism of fatigue crack growth in rubbers under severe loading: the effect of stress-induced crystallization. Macromolecules 2010;43:4708–14. http://dx.doi.org/10.1021/ma100042n.

[9] Kalay G, Bevis MJ. Processing and physical property relationships in injection-molded isotactic polypropylene. 2. Morphology and crystallinity. J Polym Sci Part B Polym Phys 1997;35:265–91. http://dx.doi.org/10.1002/(SICI)1099-0488(19970130)35:2<265::AID-POLB6>3.0.CO;2-R.

[10] Toki S, Fujimaki T, Okuyama M. Strain-induced crystallization of natural rubber as detected real-time by wide- angle X-ray diffraction technique. Polymer (Guildf) 2000;41:5423–9. http://dx.doi.org/10.1016/S0032-3861(99)00724-7.

[11] Toki S, Sics I, Ran S, Liu L, Hsiao BS. Molecular orientation and structural development in vulcanized polyisoprene rubbers during uniaxial deformation by in situ synchrotron X-ray diffraction. Polymer (Guildf) 2003;44:6003–11. http://dx.doi.org/10.1016/S0032-3861(03)00548-2.

[12] Ikeda Y, Yasuda Y, Makino S, Yamamoto S, Tosaka M, Senoo K, Kohjiya S. Strain-induced crystallization of peroxide-crosslinked natural rubber. Polymer (Guildf) 2007;48:1171–5. http://dx.doi.org/10.1016/j.polymer.2007.01.006.

[13] Toki S, Sics I, Ran S, Liu L, Hsiao BS, Murakami S, Senoo K, Kohjiya S. New insights into structural development in natural rubber during uniaxial deformation by in situ synchrotron X-ray diffraction. Macromolecules 2002;35:6578–84. http://dx.doi.org/10.1021/ma0205921.

[14] Toki S, Sics I, Hsiao BS, Tosaka M, Poompradub S, Ikeda Y, Kohjiya S. Probing the nature of strain-induced crystallization in polyisoprene rubber by combined thermomechanical and in situ x-ray diffraction techniques. Macromolecules 2005;38:7064–73. http://dx.doi.org/10.1021/ma050465f.

[15] Hernández M, López-Manchado MA, Sanz A, Nogales A, Ezquerra TA. Effects of strain-induced crystallization on the segmental dynamics of vulcanized natural rubber. Macromolecules 2011;44:6574–80. http://dx.doi.org/10.1021/ma201021q.

[16] Gorlier E, Haudin JM, Billon N. Strain-induced crystallisation in bulk amorphous PET under uni-axial loading. Polymer (Guildf) 2001;42:9541–9. http://dx.doi.org/10.1016/S0032-3861(01)00497-9.

[17] Luch D, Yeh GSY. Morphology of strain-induced crystallization of natural rubber. Part II. X-Ray studies on cross-linked vulcanizates. J Macromol Sci Part B Phys 1973;7:121–55. http://dx.doi.org/10.1080/00222347308212577.

[18] Murakami S, Senoo K, Toki S, Kohjiya S. Structural development of natural rubber during uniaxial stretching by in situ wide angle x-ray diffraction using a synchrotron radiation. Polymer (Guildf) 2002;43:2117−20. http://dx.doi.org/10.1016/S0032-3861(01)00794-7.

[19] Daver F, Blake A, Cakmak M. Stages of structural ordering leading to stress induced crystallization of PEEK films: a mechano-optical study on deformation, relaxation and retraction. Macromolecules 2009;42:2626−33. http://dx.doi.org/10.1021/ma802041n.

[20] Wu J, Schultz JM, Samon JM, Pangelinan AB, Chuah HH. In situ study of structure development in poly(trimethylene terephthalate) fibers during stretching by simultaneous synchrotron small- and wide-angle X-ray scattering. Polymer (Guildf) 2001;42:7141−51. http://dx.doi.org/10.1016/S0032-3861(01)00042-8.

[21] An H, Li X, Geng Y, Wang Y, Wang X, Li A, Li Z, Yang C. Shear-induced conformational ordering, relaxation, and crystallization of isotactic polypropylene. J Phys Chem B 2008;112:12256−62. http://dx.doi.org/10.1021/jp802511b.

[22] Lizundia E, Larranaga A, Vilas JL, Leon LM. Three-dimensional orientation of poly(l-lactide) crystals under uniaxial drawing. RSC Adv 2016;6:11943−51. http://dx.doi.org/10.1039/C5RA22680E.

[23] Angell CA. Relaxation in liquids, polymers and plastic crystals − strong/fragile patterns and problems. J Non Cryst Sol 1991;131−133:13−31. http://dx.doi.org/10.1016/0022-3093(91)90266-9.

[24] Bohmer R, Ngai KL, Angell CA, Plazek DJ. Nonexponential relaxations in strong and fragile glass formers. J Chem Phys 1993;99:4201. http://dx.doi.org/10.1063/1.466117.

[25] Roland CM, Ngai KL. Normalization of the temperature dependence of segmental relaxation times. Macromolecules 1992;25:5765−8. http://dx.doi.org/10.1021/ma00047a030.

[26] Sanz A, Nogales A, Ezquerra TA, Soccio M, Munari A, Lotti N. Cold crystallization of poly(trimethylene terephthalate) as revealed by simultaneous WAXS, SAXS, and dielectric spectroscopy. Macromolecules 2010;43:671−9. http://dx.doi.org/10.1021/ma902188c.

[27] Gupta VB, Radhakrishnan J, Sett SK. Interaction between thermal shrinkage and crystallization in axially oriented poly(ethylene terephthalate) fibres and films. Polymer (Guildf) 1993;34:3814−22. http://dx.doi.org/10.1016/0032-3861(93)90505-5.

[28] Pearce R, Cole KC, Ajji A, Dumoulin MM. Studies of post drawing relaxation phenomena in poly(ethylene terephthalate) by infrared spectroscopy. Polym Eng Sci 1997;37:1795−800. http://dx.doi.org/10.1002/pen.11828.

[29] Matthews RG, Ajji A, Dumoulin MM, Prud'Homme RE. The effects of stress relaxation on the structure and orientation of tensile drawn poly(ethylene terephthalate). Polymer (Guildf) 2000;41:7139−45. http://dx.doi.org/10.1016/S0032-3861(00)00052-5.

[30] Hassan MK, Cakmak M. Strain-induced crystallization during relaxation following biaxial stretching of PET films: a real-time mechano-optical study. Macromolecules 2015;48:4657−68. http://dx.doi.org/10.1021/acs.macromol.5b00388.

[31] Andjelić S, Scogna RC. Polymer crystallization rate challenges: the art of chemistry and processing. J Appl Polym Sci 2015;132. http://dx.doi.org/10.1002/app.42066.n/a−n/a.

[32] Lagasse RR, Maxwell B. An experimental study of the kinetics of polymer crystallization during shear flow. Polym Eng Sci 1976;16:189−99. http://dx.doi.org/10.1002/pen.760160312.

[33] Rao IJ, Rajagopal KR. Study of strain-induced crystallization of polymers. Int J Sol Struct 2001;38:1149–67. http://dx.doi.org/10.1016/S0020-7683(00)00079-2.
[34] Fernandez-Ballester L, Thurman DW, Zhou W, Kornfield JA. Effect of long chains on the threshold stresses for flow-induced crystallization in iPP: Shish Kebabs vs Sausages. Macromolecules 2012;45:6557–70. http://dx.doi.org/10.1021/ma3000384.
[35] Jabarin SA. Strain-induced crystallization of poly(ethylene terephthalate). Polym Eng Sci 1992;32:1341–9. http://dx.doi.org/10.1002/pen.760321802.
[36] Stein RS, Rhodes MB. Photographic light scattering by polyethylene films. J Appl Phys 1960;31:1873–84. http://dx.doi.org/10.1063/1.1735468.
[37] Wang Z, Ma Z, Li L. Flow-induced crystallization of polymers: molecular and thermodynamic considerations. Macromolecules 2016;49:1505–17. http://dx.doi.org/10.1021/acs.macromol.5b02688.
[38] Murase H, Ohta Y, Hashimoto T. A new scenario of shish-kebab formation from homogeneous solutions of entangled polymers: visualization of structure evolution along the fiber spinning line. Macromolecules 2011;44:7335–50. http://dx.doi.org/10.1021/ma2008817.
[39] Somani RH, Hsiao BS, Nogales A, Srinivas S, Tsou AH, Sics I, Balta-Calleja FJ, Ezquerra TA. Structure development during shear flow-induced crystallization of i-PP: in-situ small-angle X-ray scattering study. Macromolecules 2000;33:9385–94. http://dx.doi.org/10.1021/ma001124z.
[40] Tian N, Zhou W, Cui K, Liu Y, Fang Y, Wang X, Liu L, Li L. Extension flow induced crystallization of poly(ethylene oxide). Macromolecules 2011;44:7704–12. http://dx.doi.org/10.1021/ma201263z.
[41] Zuidema H, Peters GWM, Meijer HEH. Development and validation of a recoverable strain-based model for flow-induced crystallization of polymers. Macromol Theor Simul 2001;10:447–60. http://dx.doi.org/10.1002/1521-3919(20010601)10:5<447::AID-MATS447>3.0.CO;2-C.
[42] Custódio FJMF, Steenbakkers RJA, Anderson PD, Peters GWM, Meijer HEH. Model development and validation of crystallization behavior in injection molding prototype flows. Macromol Theor Simul 2009;18:469–94. http://dx.doi.org/10.1002/mats.200900016.
[43] Doufas AK, McHugh AJ, Miller C. Simulation of melt spinning including flow-induced crystallization. Part I. Model development and predictions. J Non-Newtonian Fluid Mech 2000;92:27–66. http://dx.doi.org/10.1016/S0377-0257(00)00088-4.
[44] Doufas AK, Dairanieh IS, McHugh AJ. A continuum model for flow-induced crystallization of polymer melts. J Rheol (N.Y.) 1999;43:85. http://dx.doi.org/10.1122/1.550978.
[45] Cui K, Meng L, Tian N, Zhou W, Liu Y, Wang Z, He J, Li L. Self-acceleration of nucleation and formation of shish in extension-induced crystallization with strain beyond fracture. Macromolecules 2012;45:5477–86. http://dx.doi.org/10.1021/ma300338c.
[46] Wang Y, Wang S-Q. From elastic deformation to terminal flow of a monodisperse entangled melt in uniaxial extension. J Rheol (N.Y.) 2008;52:1275. http://dx.doi.org/10.1122/1.2995858.
[47] Wang SQ, Ravindranath S, Wang Y, Boukany P. New theoretical considerations in polymer rheology: elastic breakdown of chain entanglement network. J Chem Phys 2007;127. http://dx.doi.org/10.1063/1.2753156.

[48] Heeley EL, Fernyhough CM, Graham RS, Olmsted PD, Inkson NJ, Embery J, Groves DJ, McLeish TCB, Morgovan AC, Meneau F, Bras W, Ryan AJ. Shear-induced crystallization in blends of model linear and long-chain branched hydrogenated polybutadienes. Macromolecules 2006;39:5058−71. http://dx.doi.org/10.1021/ma0606307.
[49] Mitsuhashi S. On Polyethylene crystals grown from flowing solutions in xylene. Bull Text Res Inst 1963;66:1−9.
[50] Pennings AM, Kiel AJ. Fractionation by crystallization from solution. III on the morphology of fibrillar polyethylene crystals grown in solution. Kolloid Z Z Polym 1965;205:160−2.
[51] Binsbergen FL. Orientation-induced nucleation in polymer crystallization. Nature 1966;211:516−7. http://dx.doi.org/10.1038/211516a0.
[52] De Gennes PG. Coil-stretch transition of dilute flexible polymers under ultrahigh velocity gradients. J Chem Phys 1974;60:5030−42. http://dx.doi.org/10.1063/1.1681018.
[53] Schroeder CM. Observation of polymer conformation hysteresis in extensional flow. Science 2003;301:1515−9. http://dx.doi.org/10.1126/science.1086070 (80-).
[54] Mackley MR, Keller A. Flow induced crystallization of polyethylene melts. Polymer (Guildf) 1973;14:16−20. http://dx.doi.org/10.1016/0032-3861(73)90073-6.
[55] Pope DP, Keller A. A study of the chain extending effect of elongational flow in polymer solutions. Colloid Polym Sci 1978;256:751−6. http://dx.doi.org/10.1007/BF01438032.
[56] Farrell CJ, Keller A, Miles MJ, Pope DP. Conformational relaxation time in polymer solutions by elongational flow experiments − 1. Determination of extensional relaxation time and its molecular weight dependence. Polymer (Guildf) 1980;21:1292−4. http://dx.doi.org/10.1016/0032-3861(80)90195-0.
[57] Keller HWHKA. Processing of polymers. Wiley-VCH; 1997.
[58] Zheng H, Quan Y, Zheng G, Dai K, Liu C, Shen C. Fabrication of a polymer/aligned shish-kebab composite: microstructure and mechanical properties. RSC Adv 2015;5:60392−400. http://dx.doi.org/10.1039/C5RA07453C.
[59] Yan T, Zhao B, Cong Y, Fang Y, Cheng S, Li L, Pan G, Wang Z, Li X, Bian F. Critical strain for shish-kebab formation. Macromolecules 2010;43:602−5. http://dx.doi.org/10.1021/ma9020642.
[60] Keum JK, Zuo F, Hsiao BS. Formation and stability of shear-induced shish-kebab structure in highly entangled melts of UHMWPE/HDPE blends. Macromolecules 2008;41:4766−76. http://dx.doi.org/10.1021/ma800063e.
[61] Zuo F, Keum JK, Yang L, Somani RH, Hsiao BS. Thermal stability of shear-induced shish-kebab precursor structure from high molecular weight polyethylene chains. Macromolecules 2006;39:2209−18. http://dx.doi.org/10.1021/ma052340g.
[62] Okamoto M, Kubo H, Kotaka T. Elongational flow-induced crystallization and structure development in supercooled poly(ethylene naphthalate). Macromolecules 1998;31:4223−31. http://dx.doi.org/10.1021/ma971713d.
[63] Kumaraswamy G, Issaian AM, Kornfield JA. Shear-enhanced crystallization in isotactic polypropylene. 1. Correspondence between in situ rheo-optics and ex situ structure determination. Macromolecules 1999;32:7537−47. http://dx.doi.org/10.1021/ma990772j.
[64] Seki M, Thurman DW, Oberhauser JP, Kornfield JA. Shear-mediated crystallization of isotactic polypropylene: the role of long chain-long chain overlap. Macromolecules 2002;35:2583−94. http://dx.doi.org/10.1021/ma011359q.

[65] Varga J, Karger-Kocsis J. Rules of supermolecular structure formation in sheared isotactic polypropylene melts. J Polym Sci Part B Polym Phys 1996;34:657−70. doi:papers://590F92D9-0B76-4B88-8729-9AF064BE5AC8/Paper/p2692.

[66] Sun X, Li H, Zhang X, Wang D, Schultz JM, Yan S. Effect of matrix molecular mass on the crystallization of β-form isotactic polypropylene around an oriented polypropylene fiber. Macromolecules 2010;43:561−4. http://dx.doi.org/10.1021/ma9019784.

[67] Meaurio E, Martinez De Arenaza I, Lizundia E, Sarasua JR. Analysis of the C=O stretching band of the α-crystal of poly(L-lactide). Macromolecules 2009;42:5717−27. http://dx.doi.org/10.1021/ma9008109.

[68] Yamamoto M, White JL. Theory of deformation and strain-induced crystallization of an elastomeric network polymer. J Polym Sci Part A-2 Polym Phys 1971;9:1399−415. http://dx.doi.org/10.1002/pol.1971.160090804.

[69] Shen D, Long F, Wen Z, Qian R. Conformational changes of amorphous poly(ethylene terephthalate) films during uniaxial stretching. Macromol Chem Phys 1991;192:301−7. http://dx.doi.org/10.1002/macp.1991.021920212.

[70] Ajji A, Guèvremont J, Cole KC, Dumoulin MM. Orientation and structure of drawn poly(ethylene terephthalate). Polymer (Guildf) 1996;37:3707−14. http://dx.doi.org/10.1016/0032-3861(96)00175-9.

[71] Vasanthan N, Manne NJ. Strain-induced crystallization and conformational transition of poly(trimethylene terephthalate) films during uniaxial deformation probed by polarized infrared spectroscopy. Ind Eng Chem Res 2013;52:12596−603. http://dx.doi.org/10.1021/ie401783y.

[72] Liu G, Zhang X, Wang D. Stress induced reversible crystal transition in polymers. Polym Int 2015;64:951−6. http://dx.doi.org/10.1002/pi.4903.

[73] Wu J, Schultz JM, Samon JM, Pangelinan AB, Chuah HH. In situ study of structure development during continuous hot-drawing of poly(trimethylene terephthalate) fibers by simultaneous synchrotron small- and wide-angle X-ray scattering. Polymer (Guildf) 2001;42:7161−70. http://dx.doi.org/10.1016/S0032-3861(01)00045-3.

[74] Che J, Burger C, Toki S, Rong L, Hsiao BS, Amnuaypornsri S, Sakdapipanich J. Crystal and crystallites structure of natural rubber and synthetic cis-1,4-polyisoprene by a new two dimensional wide angle x-ray diffraction simulation Method. I. Strain-induced crystallization. Macromolecules 2013;46:4520−8. http://dx.doi.org/10.1021/ma400420k.

[75] Keum JK, Kim J, Lee SM, Song HH, Son YK, Choi JI, Im SS. Crystallization and transient mesophase structure in cold-drawn PET fibers. Macromolecules 2003;36:9873−8. http://dx.doi.org/10.1021/ma034694i.

[76] Ward IM, Sweeney J. An introduction to the mechanical properties of solid polymers. 2004. http://dx.doi.org/10.1002/1521-3773(20010316)40:6<9823::AID-ANIE9823>3.3.CO;2-C.

[77] Cornish K. Chemistry, manufacture and applications of natural rubber. 2014. http://dx.doi.org/10.1533/9780857096913.1.3.

[78] Tosaka M. A route for the thermodynamic description of strain-induced crystallization in sulfur-cured natural rubber. Macromolecules 2009;42:6166−74. http://dx.doi.org/10.1021/ma900954c.

[79] Che J, Burger C, Toki S, Rong L, Hsiao BS, Amnuaypornsri S, Sakdapipanich J. Crystal and crystallites structure of natural rubber and peroxide-vulcanized natural rubber by a two-dimensional wide-angle x-ray diffraction simulation method. II. Strain-induced crystallization versus temperature-induced crystallization. Macromolecules 2013;46:9712−21. http://dx.doi.org/10.1021/ma401812s.

[80] Considère A. Annales des Ponts et Chaussées 9. 1885. p. 574–775.
[81] Toki S, Che J, Rong L, Hsiao BS, Amnuaypornsri S, Nimpaiboon A, Sakdapipanich J. Entanglements and networks to strain-induced crystallization and stress–strain relations in natural rubber and synthetic polyisoprene at various temperatures. Macromolecules 2013;46:5238–48. http://dx.doi.org/10.1021/ma400504k.
[82] Mahendrasingam A, Martin C, Fuller W, Blundell DJ, Oldman RJ, Harvie JL, MacKerron DH, Riekel C, Engström P. Effect of draw ratio and temperature on the strain-induced crystallization of poly(ethylene terephthalate) at fast draw rates. Polymer (Guildf) 1999;40:5553–65. http://dx.doi.org/10.1016/S0032-3861(98)00770-8.
[83] Chuah HH. Orientation and structure development in poly(trimethylene terephthalate) tensile drawing. Macromolecules 2001;34:6985–93. http://dx.doi.org/10.1021/ma010317z.
[84] Jabbarzadeh A, Tanner RI. Flow-induced crystallization: unravelling the effects of shear rate and strain. Macromolecules 2010;43:8136–42. http://dx.doi.org/10.1021/ma100985x.
[85] Lee HS, Park SC, Kim YH. Structural changes of poly(trimethylene terephthalate) film upon uniaxial and biaxial drawing. Macromolecules 2000;33:7994–8001. http://dx.doi.org/10.1021/ma990775w.
[86] Kokturk G, Piskin E, Serhatkulu TF, Cakmak M. Evolution of phase behavior and orientation in uniaxially deformed polylactic acid films. Polym Eng Sci 2002;42:1619–28. http://dx.doi.org/10.1002/pen.11057.
[87] Kim I-H, Lee SC, Jeong YG. Tensile behavior and structural evolution of poly(lactic acid) monofilaments in glass transition region. Fibers Polym 2009;10:687–93. http://dx.doi.org/10.1007/s12221-010-0687-6.
[88] Lee JK, Lee KH, Jin BS. Structure development and biodegradability of uniaxially stretched poly(L-lactide). Eur Polym J 2001;37:907–14. http://dx.doi.org/10.1016/S0014-3057(00)00213-5.
[89] Wong YS, Stachurski ZH, Venkatraman SS. Orientation and structure development in poly(lactide) under uniaxial deformation. Acta Mater 2008;56:5083–90. http://dx.doi.org/10.1016/j.actamat.2008.06.027.
[90] Pluta M, Galeski A. Plastic deformation of amorphous poly(L/DL-lactide): structure evolution and physical properties. Biomacromolecules 2007;8:1836–43.
[91] Hamonic F, Miri V, Saiter A, Dargent E. Rigid amorphous fraction versus oriented amorphous fraction in uniaxially drawn polyesters. Eur Polym J 2014;58:233–44. http://dx.doi.org/10.1016/j.eurpolymj.2014.06.014.
[92] Capaccio G, Ward IM. Properties of ultra-high modulus linear polyethylenes. Nat Phys Sci 1973;243:143.
[93] Capaccio G, Ward IM. Polyethylenes: effect of molecular weight and behaviour and mechanical properties. Polymer 1974;15:233–8.
[94] Hallam MA, Cansfield DLM, Ward IM, Pollard G. A study of the effect of molecular weight on the tensile strength of ultra-high modulus polyethylenes. J Mater Sci 1986;21:4199–205. http://dx.doi.org/10.1007/BF01106531.
[95] Jarecki L, Meier DJ. Ultra-high modulus polyethylene. 1 Effect of drawing temperature. Polymer (Guildf) 1979;20:1078–82. http://dx.doi.org/10.1016/0032-3861(79)90297-0.
[96] Gerrits NJA, Young RJ, Lemstra PJ. Tensile properties of biaxially drawn polyethylene. Polymer (Guildf) 1990;31:231–6. http://dx.doi.org/10.1016/0032-3861(90)90111-B.

[97] Weeks NE, Porter RS. Mechanical properties of ultra-oriented polyethylene. J Polym Sci Part B Polym Phys 1974;12:635–43.
[98] Wills AJ, Capaccio G, Ward IM. Plastic deformation of polypropylene: effect of molecular weight on drawing behavior and structural characteristics of ultra-high-modulus products. J Polym Sci Polym Phys Ed 1980;18:493–509. http://dx.doi.org/10.1002/pol.1980.180180309.
[99] Brew B, Ward IM. Study of the production of ultra-high modulus polyoxymethylene by tensile drawing at high temperatures. Polymer (Guildf) 1978;19:1338–44. http://dx.doi.org/10.1016/0032-3861(78)90319-1.
[100] Hyon S-H, Jin F, Jamshidi K, Tsutsumi S, Kanamoto T. Biodegradable ultra high strength poly(L-lactide) rods for bone fixation. Macromol Symp 2003;197:355–68. http://dx.doi.org/10.1002/masy.200350731.
[101] Polyakova A, Stepanov EV, Sekelik D, Schiraldi DA, Hiltner A, Baer E. Effect of crystallization on oxygen-barrier properties of copolyesters based on ethylene terephthalate. J Polym Sci Part B Polym Phys 2001;39:1911–9. http://dx.doi.org/10.1002/polb.1165.
[102] Liu RYF, Hu YS, Hibbs MR, Collard DM, Schiraldi DA, Hiltner A, Baer E. Improving oxygen barrier properties of poly(ethylene terephthalate) by incorporating isophthalate. I. Effect of orientation. J Appl Polym Sci 2005;98:1615–28. http://dx.doi.org/10.1002/app.22213.
[103] Özen I, Bozoklu G, Dalgiçdir C, Yücel O, Ünsal E, Çakmak M, Menceloğlu YZ. Improvement in gas permeability of biaxially stretched PET films blended with high barrier polymers: the role of chemistry and processing conditions. Eur Polym J 2010;46:226–37. http://dx.doi.org/10.1016/j.eurpolymj.2009.10.027.
[104] Wu W, Wagner MH, Qian Q, Pu W, Kheirandish S. Morphology and barrier mechanism of biaxially oriented poly(ethylene terephthalate)/poly(ethylene 2,6-naphthalate) blends. J Appl Polym Sci 2006;101:1309–16. http://dx.doi.org/10.1002/app.22728.
[105] Sekelik DJ, Stepanov EV, Nazarenko S, Schiraldi D, Hiltner A, Baer E. Oxygen barrier properties of crystallized and talc-filled poly(ethylene terephthalate). J Polym Sci Part B Polym Phys 1999;37:847–57. http://dx.doi.org/10.1002/(SICI)1099-0488(19990415)37:8<847::AID-POLB10>3.0.CO;2–3.
[106] Liu RYF, Hiltner A, Baer E. Free volume and oxygen transport in cold-drawn polyesters. J Polym Sci Part B Polym Phys 2004;42:493–504. http://dx.doi.org/10.1002/polb.10684.
[107] Michaels AS, Vieth WR, Barrie JA. Solution of gases in polyethylene terephthalate. J Appl Phys 1963;34:1–12. http://dx.doi.org/10.1063/1.1729066.
[108] Orchard GJ, Spiby P, Ward IM. Oxygen and water-vapor diffusion through biaxially oriented poly(ethylene terephthalate). J Polym Sci Part B Polym Phys 1990;28:603–21.
[109] Natu AA, Lofgren EA, Jabarin SA. Effect of morphology on barrier properties of poly(ethylene terephthalate). Polym Eng Sci 2005;45:400–9. http://dx.doi.org/10.1002/pen.20288.
[110] Liu RYF, Schiraldi DA, Hiltner A, Baer E. Oxygen-barrier properties of cold-drawn polyesters. J Polym Sci Part B Polym Phys 2002;40:862–77. http://dx.doi.org/10.1002/polb.10149.

[111] Slee JA, Orchard GAJ, Bower DI, Ward IM. Transport of oxygen through oriented poly(ethylene terephthalate). J Polym Sci Part B Polym Phys 1989;27:71−83. http://dx.doi.org/10.1002/polb.1989.090270105.
[112] Liu RYF, Hu YS, Schiraldi DA, Hiltner A, Baer E. Crystallinity and oxygen transport properties of PET bottle walls. J Appl Polym Sci 2004;94:671−7. http://dx.doi.org/10.1002/app.20905.
[113] Lin J, Shenogin S, Nazarenko S. Oxygen solubility and specific volume of rigid amorphous fraction in semicrystalline poly(ethylene terephthalate). Polymer (Guildf) 2002;43:4733−43. http://dx.doi.org/10.1016/S0032-3861(02)00278-1.
[114] El Mohajir B, Heymans N. Changes in structural and mechanical behaviour of PVDF with processing or thermal treatment. 2. Evolution of mechanical behaviour. Polymer (Guildf) 2001;42:5661−7. http://dx.doi.org/10.1016/S0032-3861(01)00184-7.
[115] Martins P, Lopes AC, Lanceros-Mendez S. Electroactive phases of poly(vinylidene fluoride): determination, processing and applications. Prog Polym Sci 2014;39:683−706. http://dx.doi.org/10.1016/j.progpolymsci.2013.07.006.
[116] Gregorio R. Effect of crystalline phase, orientation and temperature on the dielectric properties of poly (vinylidene fluoride) (PVDF). J Mater Sci 1999;4:4489−500. http://dx.doi.org/10.1023/A:1004689205706.
[117] Dmitriev IY, Lavrentyev VK, Elyashevich GK. Polymorphic transformations in poly(vinylidene fluoride) films during orientation. Polym Sci Ser A 2006;48:272−7. http://dx.doi.org/10.1134/S0965545X06030084.
[118] Sajkiewicz P, Wasiak A, Gocłowski Z. Phase transitions during stretching of poly(vinylidene fluoride). Eur Polym J 1999;35:423−9. http://dx.doi.org/10.1016/S0014-3057(98)00136-0.
[119] Salimi A, Yousefi AA. FTIR studies of β-phase crystal formation in stretched PVDF films. Polym Test 2003;22:699−704. http://dx.doi.org/10.1016/S0142-9418(03)00003-5.
[120] Li L, Zhang M, Rong M, Ruan W. Studies on the transformation process of PVDF from α to β phase by stretching. RSC Adv 2014;4:3938. http://dx.doi.org/10.1039/c3ra45134h.
[121] Matsushige K, Nagata K, Imada S, Takemura T. The II-I crystal transformation of poly(vinylidene fluoride) under tensile and compressional stresses. Polymer 1980;21:1391−7.
[122] Hsu T, Geil PH. Deformation and transformation mechanisms of poly(vinylidene fluoride) (PVF2). (n.d.) 24.
[123] McGrath JC, Ward IM. High effective draw as a route to increased stiffness and electrical response in poly(vinylidene fluoride). Elsevier; 1980. http://dx.doi.org/10.1016/0032-3861(80)90237-2.
[124] Sencadas V, Gregorio R, Lanceros-Mendez S. α to β phase transformation and microestructural changes of PVDF films induced by uniaxial stretch. J Macromol Sci Part B 2009;48:514−25. http://dx.doi.org/10.1080/00222340902837527.
[125] Gomes J, Serrado Nunes J, Sencadas V, Lanceros-Mendez S. Influence of the β-phase content and degree of crystallinity on the piezo- and ferroelectric properties of poly(-vinylidene fluoride). Smart Mater Struct 2010;19:65010. http://dx.doi.org/10.1088/0964-1726/19/6/065010.

FURTHER READING

[1] Asano T, Seto T. Morphological studies of cold drawn poly(ethylene terephthalate). Polym J 1973;5:72−85. http://dx.doi.org/10.1295/polymj.5.72.

[2] Sirota EB. Polymer crystallization: metastable mesophases and morphology. Macromolecules 2007;40:1043−8. http://dx.doi.org/10.1021/ma0615147.

[3] Seguela R. On the strain-induced crystalline phase changes in semi-crystalline polymers: mechanisms and incidence on the mechanical properties. J Macromol Sci Part C Polym Rev 2005;45:263−87. http://dx.doi.org/10.1081/MC-200067727.

[4] Stoclet G, Seguela R, Lefebvre JM, Rochas C. New insights on the strain-induced mesophase of poly(d,l-lactide): in situ WAXS and DSC study of the thermo-mechanical stability. Macromolecules 2010;43:7228−37. http://dx.doi.org/10.1021/ma101430c.

[5] Wilchinsky ZW. Measurement of orientation in polypropylene film. J Appl Phys 1960; 31:1969−72. http://dx.doi.org/10.1063/1.1735481.